Berberine dimers as chemical probes of *Pseudomonas aeruginosa* MexXY-OprM efflux function and inhibition

Logan G. Kavanaugh[1#], Andrew R. Mahoney[2#], Debayan Dey[1], William M. Wuest[2,3*] and Graeme L. Conn[1,3*]

[1]Department of Biochemistry, Emory University School of Medicine, Atlanta, GA

[2]Department of Chemistry, Emory University, Atlanta, GA

[3]Emory Antibiotic Resistance Center, Emory University, Atlanta, GA

[#]Co-first authors

*Correspondence to: Graeme L. Conn, gconn@emory.edu or William M. Wuest, wwuest@emory.edu

Keywords

Pseudomonas, antibiotic, efflux, Resistance-Nodulation-Division (RND), berberine, efflux pump inhibitor, MexXY-OprM.

Abbreviations

4,6-DOS, 4,6-deoxysteptamine; **CA-MHB**, cation-adjusted Mueller Hinton broth; **DPB**, Distal binding pocket; **EPI**, efflux pump inhibitor; **FIC**, fractional inhibitory concentration; **HTVS**, high-throughput virtual screening; **PBP**, proximal binding pocket; PEG, polyethylene glycol; **RND**, Resistance-Nodulation-Division. *Antibiotics*: **Ami**, amikacin; **Cef**, cefepime; **Cip**, ciprofloxacin; **Gen**, gentamicin; **Kan**, kanamycin; **Imi**, imipenem; **Tig**, tigecycline; **Tob**, tobramycin.

Abstract

The Resistance-Nodulation-Division (RND) efflux pump superfamily is pervasive among Gram-negative pathogens and contributes extensively to clinical antibiotic resistance. The opportunistic pathogen *Pseudomonas aeruginosa* contains 12 RND-type efflux systems, with four contributing to resistance including MexXY-OprM which is uniquely able to export aminoglycosides. At the site of initial substrate recognition, small molecule probes of the inner membrane transporter (e.g., MexY) have potential as important functional tools to understand substrate selectivity and a foundation for developing adjuvant efflux pump inhibitors (EPIs). Here, we optimized the scaffold of berberine, a known but weak MexY EPI, using an *in-silico* high-throughput screen to identify berberine dimers with enhanced synergistic action with aminoglycosides. Further, docking and molecular dynamics simulations of berberine dimers reveal unique contact residues and thus sensitivities of MexY from distinct *P. aeruginosa* strains. This work thereby reveals berberine dimers to be useful probes of MexY transporter function and potential leads for EPI development.

Introduction

Multi-drug resistant bacteria pose a global health threat with escalating infection cases resulting in increased morbidity and mortality, longer hospital stays, and increased financial burden[1,2]. In patients with cystic fibrosis, chronic lung infections caused by *Pseudomonas aeruginosa* are common and eradication is challenging[3-5]. In *P. aeruginosa* and other Gram-negative pathogens, expression of the chromosomally encoded Resistance-Nodulation-Division (RND) superfamily efflux pumps contributes extensively to multidrug resistance[6-11]. However, development of efflux pump inhibitors (EPIs) as therapeutics has proven challenging and is further impacted by the more broadly slowed progression of new antibiotic discovery and development[12,13].

P. aeruginosa encodes 12 hydrophobe/ amphiphile efflux-1 (HAE-1) family efflux pumps within the RND superfamily, of which four contribute to clinical antibiotic resistance: MexAB-OprM, MexCD-OprJ, MexEF-OprN, and MexXY-OprM[7-10]. These four pumps have overlapping, yet distinct antibiotic substrate profiles with MexXY-OprM having a unique ability to recognize and efflux aminoglycoside antibiotics[14-16]. For therapeutic regimes requiring aminoglycoside use, such as inhaled tobramycin for treatment of cystic fibrosis-associated *P. aeruginosa* infections, the MexXY-OprM efflux system plays a crucial role in resistance development and treatment failure[17-19]. A deeper understanding of the mechanisms governing antibiotic recognition by RND systems and the development of small molecule EPIs are urgently needed to negate efflux-mediated antibiotic resistance.

RND efflux pumps are tripartite protein complexes comprising a homotrimeric outer membrane channel (e.g., OprM), homohexameric periplasm adaptor protein (e.g., MexX), and a homotrimeric inner membrane transporter (e.g., MexY; **Fig. 1a**)[20-22]. The inner membrane transporter is a substrate/ H^+ antiporter and is the initial site for substrate recognition. Each protomer of the trimeric inner membrane

transporter contains 12 transmembrane helices (TM1-TM12) and a periplasmic domain with six subdomains that comprise the pore (PN1, PN2, PC1, PC2) and the MexX docking interface (DN, DC) (**Fig. 1b**)[23-26]. Two main predicted entry channels from the periplasmic space into the transporter are the cleft, between PC1 and PC2 of a single protomer, and the vestibule, between PN2 of one protomer and PC2 of a second protomer (**Fig. 1b**)[18,24]. Each protomer cycles through three conformational states that are required for substrate entry into the transporter and subsequent translocation to the channel of the periplasmic adapter: access, binding, and extrusion[24,25,27]. Potential efflux substrates first enter the proximal binding pocket (PBP) of the access state located within PC1 and PC2 and activate a conformational change at the glycine-rich "switch loop" (**Fig. 1b**)[28]. Substrates then move to the distal binding pocket (DBP) as the transporter cycles to the binding and then extrusion states for release of substrate to the open efflux tunnel. However, specific residues within the PBP and DBP required for substrate recognition and conformational state change have yet to be elucidated.

To provide insight into substrate recognition and/ or potential EPI binding, we aimed to identify potential molecular probes with distinct binding sites in the PBP /DBP region of MexY. Using the natural isoquinoline alkaloid berberine, a specific but weak MexY EPI[29,30], as the starting scaffold in virtual screening against a homology model of MexY, we identified four novel berberine analogs. Through iterative rounds of structure-guided docking, molecular dynamics simulations, organic synthesis, and microbiological assays, we identified berberine dimers that displayed increased synergy with aminoglycosides compared to natural berberine in *P. aeruginosa* PAO1, PA7, PA14, and pan-aminoglycoside resistant clinical isolates (**Supplemental Table S1**). Through alteration of the dimer linker properties, we also demonstrate the applicability of these new berberine derivatives to identify binding pocket residues and substrate conformational properties which may play a role in specific substrate recognition by MexY.

Results

Virtual screening predicts four diverse berberine scaffolds as MexY chemical probes.

In silico high-throughput virtual screening (HTVS) in the Schrödinger software was used to predict berberine analogs with enhanced binding scores and/ or distinct binding sites within the MexY PBP and DBP. Berberine was first used as a query on PubChem to generate a custom compound set comprising ~10,000 potential ligands with a Tanimoto coefficient threshold >0.8. This ligand set was next docked using HTVS Glide (Schrödinger) into a binding pocket comprising the PBP and DBP of a *P. aeruginosa* PAO1 MexY ($MexY^{PAO1}$) homology model in its binding conformational state[31]. Ligands were ranked and the top scoring 1000 were subsequently re-docked with increased precision using Glide SP (Schrödinger). The top 1000 ligands were also clustered using a K-means algorithm based on chemical similarity to ensure selection of diverse scaffolds for further experimental investigation. This process produced four chemically

diverse ligands (**Scheme 1**, *Generation 1*): berberine conjugated with piperazine (Ber-Pip [**1**] and Ber-Carb [**2**]) or propanamine moieties (Ber-Prop [**3**]), and a berberine dimer with a hexane linker (Ber-C6 [**4**]).

Our docking model predicted berberine binding to $MexY^{PAO1}$ through multiple π-stacking interactions, including F610 in the switch loop and W177 in the DBP, as previously seen[29] (**Fig. 2a**). Furthermore, docking predicted three of the berberine analogs (Ber-Pip [1], Ber-Prop [3], Ber-C6 [4]) to have comparable or increased binding scores compared to berberine (**Supplemental Table S2**). In the DBP, Ber-Pip [**1**] and Ber-Carb [**2**] were predicted to have π-π stacking and π-cation interactions, respectively, while the terminal amino group of Ber-Prop [**3**] was positioned to interact with D124 (**Supplemental Fig. S1a-c** and **Supplemental Table S3**). Ber-C6 [**4**] was predicted to bind in the DBP at the PC1/DN interface through multiple interactions, including π-stacking with Y752, π-cation interaction with K764, hydrogen bonding with the backbone of T176, and a salt bridge formed with E273 (**Supplemental Fig. S1d** and **Supplemental Table S3**).

Berberine dimer has increased synergy with aminoglycosides.

To test the validity of our computational modeling, a semisynthetic strategy was developed to obtain the top four ligands Ber-Pip [**1**], Ber-Carb [**2**], Ber-Prop [**3**] and Ber-C6 [**4**] (**Scheme 1**–*Generation 1* and see Supplementary Methods). Synthesis began with selective C9-demethylation of commercial berberine chloride via vacuum pyrolysis to generate the natural product berberrubine chloride in high yield. The resulting phenol was appended to a commercially available tertiary amine scaffold via a carbamate linkage to give Ber-Carb [**2**]. Next, the electron-rich nature of the berberrubine ring system allowed for derivatization of C13 by double condensation of berberrubine chloride and N-methylpiperazine onto formaldehyde under acidic conditions, generating Ber-Pip [**1**]. Heating berberrubine chloride with 1,6-diiodohexane for 72 hours successfully generated the berberine dimer Ber-C6 [**4**], as well as a small amount of monohaloalkylated berberine. Because of the small amount of this isolated byproduct as well as its low reactivity, the propanamine derivative required an alternate approach in which berberrubine chloride was instead alkylated using 3-(Boc-amino)propyl bromide. Deprotection with hydrochloric acid then successfully afforded the desired ligand Ber-Prop [**3**] as the hydrochloride salt.

Checkerboard synergy assays were performed for berberine and the four synthesized analogs in *P. aeruginosa* PAO1 in the presence of two 4,6-deoxysteptamine (4,6-DOS) aminoglycosides, kanamycin (Kan) and gentamicin (Gen) (**Fig. 1c**). Checkerboard assays confirmed berberine (4 μg/mL) is a weak inhibitor of the MexXY-OprM efflux pump, reducing the minimum inhibitory concentration (MIC) by two-fold and with a fractional inhibitory concentration (FIC) of 0.5, where FIC values < 0.5 are considered synergistic (**Fig. 1c**, **Table 1**, and **Supplemental Table S4**). As MICs for berberine and analogs could not be experimentally determined, FIC value calculations used estimated MICs obtained via nonlinear regression of final culture OD_{600} (see Methods). Ber-Prop [**3**] and Ber-C6 [**4**] showed increased synergy with Kan and Gen, with Ber-C6 [**4**] reducing the MIC two- to six-fold (FIC = 0.28-0.51). However, growth inhibition was observed in the presence of Ber-C6 [**4**] alone suggesting aminoglycoside-independent growth inhibition

(**Fig. 1c**, **Table 1**, and **Supplemental Table S4**). Piperazine ligands, Ber-Pip [**1**] and Ber-Carb [**2**] showed weaker or no synergy with the two aminoglycosides tested (**Fig. 1c**,**Table 1**, and **Supplemental Table S4**). As a result, we selected the berberine dimer, Ber-C6 [**4**], as our focus for further development (**Scheme 1**–*Generation 2*) due to its increased aminoglycoside synergism, higher predicted binding score, and more extensive and diverse predicted interactions within the DBP of $MexY^{PAO1}$.

***Berberine alkane linker length defines MexXY-OprM inhibition efficacy and specificity*.**

Berberine dimers were designed with systematic variation in alkyl chain length connecting the two berberine groups to assess the role of linker length, flexibility, and overall size of the dimeric scaffold in predicted binding and MexXY-OprM inhibition. These *Generation 2* ligands with propane (Ber-C3 [**5**]), butane (Ber-C4 [**6**]), octane (Ber-C8 [**7**]), decane (Ber-C10 [**8**]), or dodecane (Ber-C12 [**9**]) linkers (**Scheme 1**) were docked in $MexY^{PAO1}$ binding pocket as before (**Fig. 2b-c**, **Supplemental Fig. S1e-g** and **Supplemental Table S2**).

An overall trend between longer linker length and increased predicted binding score was observed with the exception of the shortest alkane-linked dimer, Ber-C3 [**5**] (**Supplemental Table S2**).The predicted lowest energy docked pose for Ber-C4 [**6**] differs from Ber-C6 [**4**], with loss of hydrophobic interactions but gain of alternative stabilization via a salt bridge interaction with E175 in the DBP (**Supplemental Fig. S1e** and **Supplemental Table S3**). In contrast, the dimer with the shortest linker, Ber-C3 [**5**], is predicted to make a greater number of stabilizing interactions in the DBP through hydrogen bonding (to S46, T176 and S272), π-stacking/cation contacts (to Y127 and K291), and a salt bridge (with E273) (**Fig. 2b** and **Supplemental Table S3**). Ber-C8 [**7**] was predicted to be stabilized through hydrogen bonding interactions with S46 and K79 in the PBP, while Ber-C10 [**8**] and Ber-C12 [**9**] had predicted interactions in the DBP with overlapping (K291), and distinct residues (E175 and Y127, respectively; **Fig. 2d**, **Supplemental Fig. S1f,g** and **Supplemental Table S3**). These docking results suggest that increased linker flexibility may allow the two berberine groups to independently adopt favorable conformations resulting in optimal interactions within the binding pocket, as no direct interactions were predicted with any alkane linker. Conversely, the Ber-C3 [**5**] dimer can fortuitously adopt numerous stabilizing interactions within the DBP despite being more conformationally constrained.

Each of these new berberine dimer analogs was obtained via reaction of berberrubine chloride with commercially available alkyl dihalides (**Scheme 1**–*Generation 2* and see Supplementary Methods). Yields were moderate and increased consistently with alkyl chain length, suggesting that the dimerization reaction is slowed either by the steric repulsion of the bulky polycyclic rings or the electronic repulsion of the charged quaternary nitrogen atoms as they approach one another. This hypothesis is additionally supported by the observation that addition of a single berberrubine monomer to the alkyl halide was relatively rapid, leading to isolable monoalkylated product in less than one hour, but complete addition of a second berberrubine molecule took up to 72 hours.

145 Checkerboard synergy assays were performed using *P. aeruginosa* PAO1 with each dimer in
146 combination with Kan and Gen (**Fig. 3a** and **Supplemental Fig. S2a**). Shortening the alkane linker in Ber-
147 C3 [**5**] and Ber-C4 [**6**] reduced the MIC of Kan up to four-fold (FIC=0.30 and 0.38, respectively; **Fig. 3a**,
148 **Table 1**, **Supplemental Fig. S2a** and **Supplemental Table S4**). Additionally, Ber-C4 reduced the MIC of
149 Gen up to four-fold (FIC=0.38) (**Supplemental Fig. S2a** and **Supplemental Table S4**). Ber-C3 at 64 µg/mL
150 was able to reduce the MIC of Gen four-fold (**Table 1**), but at the highest concentration (128 µg/mL),
151 reduced the Gen MIC six-fold (FIC=0.30, **Fig. 3a**). Increasing alkane linker length resulted in increased
152 synergistic killing of PAO1 in combination with aminoglycosides, but with increased aminoglycoside-
153 independent growth inhibition. Ber-C8 [**7**] reduced the MIC of Kan and Gen four-fold (FIC=0.28) and six-
154 fold (FIC=0.38), respectively, while Ber-C10 [**8**] and Ber-C12 [**9**] reduced the MICs of both aminoglycosides
155 by six- to eight-fold (**Fig. 3a**, **Table 1**, **Supplemental Fig. S2a** and **Supplemental Table S4**).
156 Next, to assess each berberine dimer's effect on growth phase and the potential for aminoglycoside
157 specific interactions, we performed time-kill assays using *P. aeruginosa* PAO1 with two additional,
158 structurally distinct 4,6-DOS aminoglycoside substrates, amikacin (Ami) and tobramycin (Tob; **Fig. 3b**,
159 **Supplemental Fig. S3** and **Supplemental S4a,c**). These assays were done in the presence of the
160 berberine dimers with the two shortest and two longest alkane linkers at 64 µg/mL as this concentration
161 was predicted by checkerboard assays to allow differences to be observed across the range of linker
162 lengths. As for Kan and Gen, berberine reduced the MIC two-fold for both Ami and Tob, indicating that its
163 weak effect is independent of aminoglycoside substrate (**Table 1**, **Fig. 3b**, and **Supplemental Fig. S4a,c**).
164 Consistent with its modestly tighter predicted binding, Ber-C3 [**5**] reduced the MIC for Ami four-fold (to 0.25
165 µg/mL) and Tob two-fold (to 0.25 µg/mL), while Ber-C4 [**6**] MIC reduction was equivalent to berberine
166 (**Table 1**, **Fig. 3b**,and **Supplemental Fig. S4a,c**). For the longer alkyl-linked dimers, Ber-C10 [**8**] reduced
167 the MIC six-fold for both Ami and Tob, whereas Ber-C12 [**9**] reduced the MIC of Ami six-fold but the Tob
168 MIC only four-fold (**Table 1**, **Fig. 3b**, and **Supplemental Fig. S4a,c**). Confirming the aminoglycoside-
169 independent growth inhibition observed in previous checkerboard assays, growth curves of *P. aeruginosa*
170 PAO1 in the presence of Ber-C10 [**8**] and Ber-C12 [**9**] showed a considerable extension of lag-phase
171 growth switching to log-phase at 12 hours (compared to four hours) and a slower log-phase growth rate
172 (**Fig. 3b,** and **Supplemental Fig. S4a,c**).
173 The observation of altered growth patterns in the time-kill assays with PAO1 next prompted further
174 investigation of Ber-C3 [**5**], Ber-C4 [**6**], Ber-C10 [**8**], and Ber-C12 [**9**] specificity for the MexXY-OprM efflux
175 pump using equivalent experiments in a *P. aeruginosa* Δ*mexXY* strain (**Fig.3b**, **Supplementary Table S1**,
176 and **Supplementary Figure S4b,d**). Loss of functional MexXY-OprM in the absence of berberine ligands,
177 resulted in a four-fold MIC reduction for Ami and two-fold reduction for Tob (**Table 1**). The MICs for Ami
178 and Tob in the presence of Ber-C3 [**5**] or Ber-C4 [**6**] do not exceed those observed in the Δ*mexXY*
179 background suggesting these analogs with shorter alkane linkers are specific probes for the MexXY efflux
180 system (**Table 1**). This conclusion was further validated in time-kill assays where addition of either
181 compound in the Δ*mexXY* background did not alter growth patterns (**Fig. 3b** and **Supplementary Fig.**

182 **S4b,d**). Of note, the Ber-C3 [**5**] compound reduced the MIC of both aminoglycosides to *mexXY* knockout
183 levels, suggesting it may serve as a useful starting scaffold for MexXY-OprM EPIs. Consistent with
184 previous checkerboard assays, Ber-C10 [**8**] and Ber-C12 [**9**] further reduced the MIC of Ami (6-fold) and
185 Tob (6- and 4-fold, respectively) to below those observed in the absence of MexXY-OprM (**Fig.3b, Table**
186 **1,** and **Supplementary Figure S4b,d**). Additionally, inactivation of MexXY-OprM did not influence the
187 observed lag-phase extension or slower log-phase growth rate, suggesting the longer alkane dimers are
188 sensitizing the cell to aminoglycosides in both MexXY-dependent and -independent manners.
189 We considered the possibility that the longer alkane-linked dimers might be disrupting membrane
190 integrity, similar to amphipathic quaternary ammonium ligands with long hydrophobic chains[32,33]. However,
191 using a sheep erythrocyte hemolysis assay, we found no evidence that berberine, Ber-C4 [**6**], or either
192 long alkane dimer, Ber-C10 [**8**] or Ber-C12 [**9**], is hemolytic at 128 µg/mL, a concentration at which MexXY-
193 independent activity is clearly observed for the latter two analogs (**Supplemental Fig. S5a**). Further, using
194 a vancomycin susceptibility assay as a probe for membrane permeability[34] in *P. aeruginosa* PAO1 and
195 PAO1Δ*mexXY* resulted in identical vancomycin MICs with and without Ber-C12 [**9**] at 64 µg/mL, again
196 suggesting that the off-target effect(s) of this analog are not related to membrane perturbation
197 (**Supplemental Fig. S5b,c**). The true additional target of the longer alkane dimers is currently unknown
198 and an area on-going investigation.
199
200 ***Berberine and Ber-C3 [5] compete for binding in the MexY^{PAO1} DBP***
201 Our structure-guided docking and checkerboard assays suggest that berberine and Ber-C3 [**5**] are specific
202 inhibitors of the MexXY-OprM efflux system and bind at distinct but overlapping sites within the DBP (**Fig.**
203 **2a-b**). If correct, berberine and Ber-C3 [**5**] should compete for binding in the DBP and would therefore not
204 show synergistic activity in combination. Therefore, to provide an initial experimental validation of the ligand
205 docking, this idea was tested in a three-way synergy assay using a fixed concentration of berberine (64
206 µg/mL) and a range of concentrations of Ber-C3 [**5**] (128-1 µg/mL) and Ami (4-0.125 µg/mL). Consistent
207 with competition for binding, a weak antagonistic effect (two-fold increase in Ami MIC) or the same MIC as
208 berberine alone was observed at most concentrations of Ber-C3 [**5**] (1-16 and 32-64 µg/mL, respectively;
209 **Supplemental Table S5**). Only at 128 µg/mL was Ber-C3 [**5**] able to fully outcompete berberine for the
210 overlapping binding pocket and resulting in an Ami MIC equivalent to analog the alone (0.25 µg/mL;
211 **Supplemental Table S5**).
212
213 ***Linker structure plays a role in MexXY-OprM inhibition efficacy and specificity.***
214 To further define how linker length, flexibility and chemical structure impact berberine dimer activity and
215 their potential as probes of MexXY function, four additional dimers were designed with alternative linkers:
216 para-berberine substituents linked by one or two aryl groups, Ber-pAr [**10**] and Ber-Biph [**11**], respectively,
217 or by polyethylene glycol (PEG) linkers of different lengths, Ber-PEG5 [**12**] and Ber-PEG8 [**13**] (**Scheme**
218 **1**–*Generation 3*). For example, if dimer linker length is the primary determinant of efflux inhibition then

219 dimers of a similar size with different linker types should maintain similar activity (Ber-PEG5 [**10**] *vs*. Ber-
220 C4 [**6**], Ber-pAr [**12**] *vs*. Ber-C6 [**4**], Ber-PEG8 [**11**] *vs*. Ber-C8 [**7**], and Ber-Biph [**13**] *vs*. Ber-C10 [**8**]**.**
221 However, should flexibility or physico-chemical properties be critical, then conformationally more rigid aryl
222 rings and/or more hydrophilic PEG moieties should show activity differences between the alkane, aryl, and
223 PEG linkers of comparable length.

224 Computational docking of Ber-pAr [**10**], Ber-Biph [**11**], Ber-PEG5 [**12**], and Ber-PEG8 [**13**] showed
225 increased predicted binding scores for $MexY^{PAO1}$ compared to their corresponding length alkane-linked
226 dimers (**Supplemental Table S2**). Inspection of the lowest energy docking poses for the similarly sized
227 analogs revealed Ber-pAr [**10**], Ber-PEG5 [**12**], and Ber-PEG8 [**13**] have unique predicted interactions in
228 the binding pocket compared to their respective length-compared alkane-linked dimers. Ber-pAr [**10**] and
229 Ber-PEG5 [**12**] were both predicted to be stabilized by interactions spanning the PBP (via hydrogen
230 bonding to S671) and DBP (via π-cation interaction with Y127) (compare **Fig. 2d** and **Supplementary**
231 **Fig.S1d**, and **Supplementary Fig.S1** panels **e** and **i**, respectively; and see **Supplemental Table S3**).
232 Additionally, Ber-pAr [**10**] formed an additional linker-mediated π-cation interaction with K173 (**Fig. 2d** and
233 **Supplementary Table S3**). The longer PEG linker dimer, Ber-PEG8 [**13**], was predicted to be stabilized
234 only in the DBP through a π-cation interaction (with Y127) and salt bridge (with E175) (compare
235 **Supplemental Fig. S1** panels **f** and **j**; and see **Supplemental Table S3**). In contrast, Ber-Biph [**11**] shared
236 predicted interactions (via salt bridge with E175 and hydrogen bonding to K291) with its corresponding
237 length alkane-linked dimer, Ber-C10 [**8**], while gaining a linker-mediated π-cation interaction with K173 and
238 an additional salt bridge with E273 (compare **Supplemental Fig. S1** panels **g** and **h**; and see
239 **Supplemental Table S3**). To complement these computational predictions with experimental assays of
240 dimer activity, the four aryl- or PEG-linked dimers were generated by chemical synthesis as before
241 (**Scheme 1**–*Generation* 3 and see Supplementary Methods). Synthesis of these *Generation 3* PEG-ylated
242 analogs and aryl analogs proceeded similarly to the alkyl linkers over 72 hours despite the more activated
243 benzylic electrophiles in the latter.

244 Checkerboard synergy assays were performed as before using *P. aeruginosa* PAO1 in combination
245 with Kan and Gen (**Fig. 3a** and **Supplemental Fig. S2b**). Notably, increased predicted binding scores did
246 not correlate with increased aminoglycoside synergy as previously observed for *Generation 1* and
247 *Generation 2* analogs (**Table 1** and **Supplemental Table S2**). The Ber-pAr [**10**] dimer showed synergy
248 with only Gen, reducing the MIC up to four-fold (FIC = 0.33-0.52), and predicted FICs for both tested
249 aminoglycosides were greater than the comparable Ber-C6 [**4**] dimer (**Fig. 3a** and **Supplemental Table**
250 **S4**). Ber-Biph [**11**], Ber-PEG5 [**12**], and Ber-PEG8 [**13**] showed similar or decreased synergy with Kan and
251 Gen compared to berberine, resulting in FIC values substantially higher than each corresponding length
252 alkane-linked dimer (**Supplemental Fig. S2a,b** and **Supplemental Table S4**).

253 Time-kill assays in *P. aeruginosa* PAO1 showed only two-fold reduction in MIC for both Ami and
254 Tob for Ber-pAr [**10**], Ber-PEG5 [**12**], and Ber-PEG8 [**13**] which is lower than the corresponding alkyl-linked
255 dimer in each case and comparable to berberine (**Fig. 3b**, **Table 1**, and **Supplemental Fig. S4a,c**). Ber-

256 pAr [**10**] alone resulted a reduction in log-phase growth rate but neither Ber-PEG5 [**12**] nor Ber-PEG8 [**13**]
257 affected overall growth rate (**Fig. 3b** and **Supplemental Fig. S4a,c**, respectively). To assess the specificity
258 for the MexXY-OprM efflux pump, time-kill assays were performed in the isogenic Δ*mexXY* strain. While
259 no difference in growth rate was again observed in the presence of the PEG-ylated dimers, the reduced
260 log-phase growth rate in the presence of Ber-pAr [**10**] observed in PAO1 was also observed in the Δ*mexXY*
261 background (**Supplemental Fig. S4b,d** and **Fig. 3b**, respectively), suggesting this compound may exhibit
262 off-target effects. However, as for the longer alkane-linked dimers, we found no evidence for an effect on
263 membrane integrity (**Supplementary Fig. S5a**).
264 Overall, computational docking predicted increased binding affinities for *Generation 3* compounds
265 compared to their similarly sized alkane dimer analogs, but this did not result in the anticipated increased
266 synergy with aminoglycosides. We therefore propose the alkane linker flexibility may play an important role
267 in ligand uptake into MexY and subsequent entry into the PBP/ DBP.
268
269 ***Molecular dynamics (MD) simulations reveal important berberine probe characteristics.***
270 From the studies thus far, three ligands were selected as lead probes – Ber-C3 [**5**], Ber-pAr [**10**], and Ber-
271 C12 [**9**] – reflecting the highest activity identified but with distinct linker flexibility, predicted binding pocket,
272 and/ or specificity for MexXY-OprM. First, to more precisely define the nature and stability of predicted
273 interactions made by berberine and these dimeric analogs with the $MexY^{PAO1}$ DBP/ PBP, we used a 50 ns
274 MD simulation in the Schrödinger Desmond module followed by MM/GBSA calculations on selected
275 structures along the trajectory. Interestingly, berberine and Ber-C3 [**5**] showed greater overall
276 conformational flexibility over the simulation, compared to Ber-pAr [**10**] and Ber-C12 [**9**] (**Fig. 4a**). However,
277 while similar total numbers of interactions were identified for each ligand pre- and post-simulation, only
278 Ber-C3 [**5**] and Ber-pAr [**10**] maintained specific interactions over their trajectories (**Fig. 4a** and
279 **Supplemental Table S6**).
280 MM/GBSA calculations were performed on representative structures in each 10 ns window (100
281 frames) over the 50 ns simulation to obtain the relative free energy of each ligand in its binding pocket and
282 thus reveal potentially important characteristics of a MexY inhibitor (**Fig. 4b-d** and **Supplemental Fig.**
283 **S6a-c**). As expected, the overall average binding scores for Ber-C3 [**5**] (-116.0 kcal/mol), Ber-pAr [**9**] (-
284 110.8 kcal/mol), and Ber-C12 [**10**] (-128.9 kcal/mol) were significantly greater than berberine (-65.23
285 kcal/mol; **Fig. 4b**) where the total binding score is calculated from individual electrostatic, hydrogen bond,
286 π-packing (π-mediated interactions), lipophilic, Van der Waals and solvation energetic scores.
287 The dimeric berberine ligands had significantly higher electrostatic interaction contributions than
288 berberine, but there were no significant differences in hydrogen bonding contributions (**Supplemental Fig.**
289 **S6a-b**). Ber-C12 [**9**] was predicted to make significantly more lipophilic interactions in the binding pocket
290 than Ber-C3 [**5**], Ber-pAr [**10**], and berberine, which contributed to its high predicted binding affinity
291 (**Supplemental Fig. S6c**). Reflecting its increased interactions with hydrophobic residues within the DBP
292 during the MD simulation, Ber-C3 [**5**] has a significantly more favorable π-stacking mediated interactions,

293 potentially due to enhanced flexibility seen within the simulation allowing it to position optimally to interact
294 with the binding pocket (**Fig. 4a,c**). This was further validated in the ligand strain energy calculation (the
295 difference between the ligand's free energy when bound compared to free in solution), where Ber-C3 [**5**]
296 showed the lowest ligand strain energy (**Fig. 4b,d**). MD simulations of berberine and lead dimer probes
297 thus highlight characteristics, such as increased binding affinity, ability for multiple hydrophobic
298 interactions, while maintaining flexibility and overall low ligand strain, as important for the development of
299 MexXY-OprM specific efflux pump inhibitors.
300
301 ***Top berberine alkane dimers are active against P. aeruginosa PA7 and PA14.***
302 To further investigate the efficacy and utility of our top lead probes, Ber-C3 [**5**], Ber-pAr [**10**], and Ber-C12
303 [**9**], we evaluated synergy with Gen in two additional *P. aeruginosa* strains, PA7 and PA14 (**Supplemental**
304 **Table S1** and **Table 2**). Alignment of the MexY protein sequence from *P. aeruginosa* PA7 (GenBank
305 ABR84278; $MexY^{PA7}$) and PA14 (GenBank ABJ11205; $MexY^{PA14}$) with $MexY^{PAO1}$ (GenBank OP868818)
306 revealed 96.56% and 99.04% amino acid identity, respectively. This high conservation suggests that
307 berberine and all analogs should maintain comparable predicted binding to the three MexY proteins. This
308 was confirmed using SP Glide which produced binding scores that were broadly comparable to $MexY^{PAO1}$
309 for both $MexY^{PA7}$ and $MexY^{PA14}$, with only a few larger differences (> 1 kcal/mol) and generally moderately
310 tighter and weaker binding for $MexY^{PA7}$ and $MexY^{PA14}$, respectively (**Supplemental Table S2**). However,
311 mapping the unique residues between the three *P. aeruginosa* strains on our $MexY^{PAO1}$ homology model
312 reveals that while most differences reside in the docking and transmembrane domains, four are located
313 within the PBP/DBP: A589G ($MexY^{PAO1}$), D149G ($MexY^{PA7}$), S144A ($MexY^{PA7}$) and E175Q ($MexY^{PA14}$) (**Fig.**
314 **5a**). Whether these differences result in differential activity of the berberine analogs was therefore explored
315 with berberine and the three top selected dimers, Ber-C3 [**5**], Ber-pAr [**10**], and Ber-C12 [**9**].
316 Time-kill assays were performed for berberine, Ber-C3 [**5**], Ber-C12 [**9**], and Ber-pAr [**10**], at 64
317 µg/mL in combination with Gen against *P. aeruginosa* PA7 and PA14 (**Fig. 5b**). Berberine reduced the
318 MIC for Gen in PA7 two to four-fold and up to two-fold in PA14 (**Table 2** and **Fig. 5b**). Alkane-linked dimers,
319 Ber-C3 [**5**] and Ber-C12 [**9**], exhibited similar activity in each strain, reducing the Gen MIC six-fold in PA7
320 and two-fold in PA14 (**Table 2** and **Fig. 5b**). These results contrast to PAO1 where Ber-C3 [**5**] and Ber-
321 C12 [**9**] differentially reduced the MIC of Gen four-fold and eight-fold, respectively. For the aryl-linker dimer,
322 Ber-pAr [**10**] reduced the MIC of Gen four-fold in PA7, comparable to PAO1, but reduced the MIC up to 2-
323 fold in PA14. (**Table 2** and **Fig. 5b**). Overall, changes in Gen MICs in PAO1 were comparable to those
324 observed in PA7, but all ligands were less effective in PA14 (**Table 2**).
325 We next used computational docking to investigate whether any of the binding pocket residue
326 changes identified in the MexY sequence alignment (**Fig. 5a**) might be responsible for the observed
327 differences in synergism in PAO1/ PA7 compared to PA14. Docking of Ber-C3 [**5**], Ber-pAr [**10**], and Ber-
328 C12 [**9**] in homology models of $MexY^{PAO1}$, $MexY^{PA7}$, and $MexY^{PA14}$ elucidated important differences in
329 predicted binding poses of the berberine dimers, suggesting that inherent differences between each MexY

binding pocket may indeed exist (**Supplemental Fig. S7** and **S8**). In particular, a predicted interaction with MexY from three strains was observed at residue 175, i.e. $MexY^{PAO1}$/ $MexY^{PA7}$ E175 and $MexY^{PA14}$ Q175 (**Fig. 5c** and **Supplemental Fig. S7b-d**). In $MexY^{PAO1}$/ $MexY^{PA7}$, E175 extends into the binding pocket, whereas Q175 of $MexY^{PA14}$ adopts a distinct conformation resulting in potential clash with the berberine analogs (**Fig. 5c**). This observation suggests that the identity and thus positioning of the residue 175 side chain may influence the preferred ligand conformation and subsequent binding pocket interactions. For example, Ber-C3 [**5**] adopts an 'extended' conformation in $MexY^{PAO1}$/ $MexY^{PA7}$ but a 'compact' conformation in $MexY^{PA14}$, resulting in loss of important π-cation/ π- π stacking interactions (with Y127 and K291) and salt bridges (to E273 in $MexY^{PAO1}$ and E175 in $MexY^{PA7}$). These differences in interactions resulting from the change at residue 175 can thus explain the decreased fold-change in Gen MIC observed for PA14 (**Fig. 5c**, **Table 2**, and **Supplemental Fig. S7b**-**S8**). Thus, these results exemplify how berberine dimers can be used as functional probes of the MexY binding pocket to elucidate important residues involved in ligand recognition.

Berberine dimers are active against pan-aminoglycoside resistant clinical isolates and show preferential synergy with aminoglycoside substrates of MexXY-OprM

Having defined activity in *P. aeruginosa* PAO1, PA7 and PA14, we extended these studies to further explore the potential utility of the top three berberine dimer analogs by assessing efflux inhibition activity in two pan-aminoglycoside resistant *P. aeruginosa* clinical isolates, K2156 and K2161 [35] (**Supplemental Table S1**). Alignment of the MexY protein sequence from *P. aeruginosa* K2156 (GenBank OP868819; $MexY^{K2156}$) and K2161 (GenBank OP868820; $MexY^{K2161}$) with $MexY^{PAO1}$ (GenBank OP868818) revealed 99.52% and 99.62% amino acid identity, respectively. Unique residues from both clinical isolates were primarily located in the transmembrane region of the $MexY^{PAO1}$ homology model, with no observed changes in the PBP/ DBP binding pocket (**Supplemental Fig. S9**). However, both $MexY^{K2156}$ and $MexY^{K2161}$ have Q840E (cleft) and T543A (transmembrane) amino acid substitutions, with additional unique V980I (transmembrane) changes in $MexY^{K2156}$ and A33V (vestibule) and D428N (central cavity) in $MexY^{K2161}$ (**Supplemental Fig. S9**).

MIC assays were performed for clinical isolates K2156 and K2161 in the presence of 4,6-DOS aminoglycosides (Kan, Ami, Gen, and Tob) and 64 µg/mL of berberine or berberine dimer (**Table 3**). To compare berberine ligand synergy with aminoglycosides, MICs for the isogenic Δ*mexXY* knockout for each clinical isolate were also determined (**Table 3** and **Table S1**). Berberine, Ber-C3 [**5**], and Ber-pAr [**10**] exhibited increased synergy against K2156, with a six- to eight-fold reduction in all MICs, where eight-fold reduction represented complete MexXY-OprM inhibition. Ber-C12 [**9**] reduced the MIC of Kan below Δ*mexXY* knockout levels (ten-fold reduction; ; **Table 3**). Additionally, berberine and the tested berberine dimers all showed increased synergy of four to six-fold MIC reduction with Tob, which were below the two-fold reduction observed in the Δ*mexXY* background (**Table 3**). In contrast, a low to moderate change (zero to four-fold) reduction in Kan, Ami and Gen MICs was observed for K2161 in the presence of berberine

367 and berberine dimers, of which Ber-C3 [**5**] and Ber-C12 [**9**] showed increased synergy compared to
368 berberine and Ber-pAr [**10**]. Interestingly, Ber-C3 [**5**] and Ber-C12 [**9**] inhibited Tob to Δ*mexXY* knockout
369 levels (four-fold reduction), but none of the berberine compounds inhibited below observed knockout
370 levels, suggesting off-target effects may also be strain dependent (**Table 3**). The variable synergies
371 exhibited with pan-aminoglycoside clinical isolates in the presence of berberine, Ber-C3 [5], Ber-C12 [9],
372 and Ber-pAr [10] in combination with homology modeling suggests these chemical probes could potentially
373 be used to further understand efflux substrate interactions at entry channels (e.g., cleft, vestibule, central
374 cavity) into MexY.

375 Finally, to assess the ability of these dimeric berberine probes to provide insight into binding
376 preferences of other, non-aminoglycoside substrates and their routes through the MexY transporter, we
377 determined MICs for a representative panel of additional antibiotics: tigecycline (Tig), cefepime (Cef),
378 ciprofloxacin (Cip); and the non-MexY-substrate imipenem (Imi) (**Table 3**). Ber-C3 [**5**] and Ber-C12 [**9**]
379 reduced the MIC of Tig two- to four-fold in PAO1 and K2156, whereas Ber-C12 [**9**] produced only a two-
380 fold reduction in K2161 (**Table 3**). Additionally, Ber-C3 [**5**] reduced the MIC two-fold for the substrate Cef
381 in PAO1. All other interactions between non-aminoglycoside substrates (Cef or Cip), *P. aeruginosa* strains
382 (PAO1, K2156, or K2161), and ligands (berberine, Ber-C3 [**5**], Ber-C12 [**9**], or Ber-pAr [**10**]) resulted in
383 either no difference in observed MIC or an increase in resistance (**Table 3**). Such increase in resistance is
384 most likely due to increased efflux of these substrates by another RND-efflux system in *P.* aeruginosa.
385 Additionally, a two-fold decrease in the MIC of non-substrate Imi was observed in the presence of Ber-C12
386 [**9**] (PAO1 and K2161) and Ber-pAr (PAO1) (**Table 3**). These data suggest that the berberine alkyl dimers
387 can be used as aminoglycoside-specific probes for MexY efflux function across different *P. aeruginosa*
388 strains. Additionally, our berberine dimers may serve as useful tool for understanding crosstalk between
389 multiple RND systems in *Pseudomonas*.
390

391 ## Discussion

392 The development of efflux pump inhibitors (EPIs) remains challenging due to limitations in our
393 understanding of substrate recognition and efflux mechanisms, as well as the resource-intensive nature of
394 screening chemical libraries *in vitro* for potential hits[36]. Although no EPIs have progressed to clinical
395 approval, those discovered such as phenylalanine arginyl β-napthylamide (PAβN) and carbonyl cyanide-
396 m-chlorophenylhydrazone (CCCP) have provided valuable tools to study efflux function [37-41]. However,
397 these general inhibitors suffer significant limitations such as being substrates for multiple RND systems
398 within the same organism or having off-target effects, both of which limit their use as tools to study specific
399 RND efflux transporter function[41]. Therefore, we aimed to identify a pathway to new chemical probes,
400 specific for the MexXY-OprM efflux system, to elucidate efflux function and inhibition.

401 Here, based on its known MexXY-OprM EPI activity, we used the naturally occurring and well-
402 studied alkaloid berberine as a starting scaffold for a structure-guided computational screen[29,30,42-47]. HTVS

403 identified four berberine analogs (*Generation 1*) as potential leads with diverse predicted binding
404 preferences in the MexY PBP/ DPB. Among the *Generation 1* ligands, addition of piperazine moieties to
405 monomeric berberine did not enhance inhibition as previously shown for other pyridylpiperazine-based
406 allosteric inhibitors of RND efflux systems[48]. However, our studies identified an alkane-linked berberine
407 dimer, Ber-C6 [**4**], as an alternative promising lead for MexY. Berberine dimers have been shown to bind
408 preferentially to G-quadruplex DNA but, to our knowledge, have yet to be characterized as protein
409 inhibitors[49,50].

410 Using novel berberine dimers of variable linker length (*Generation 2*) and chemical nature
411 (*Generation 3*), we identified linker characteristics that affect inhibition of the MexXY-OprM efflux system.
412 Generally, alkyl linker length correlated with increased binding scores, and these predictions were
413 corroborated by biological data showing improved synergy with aminoglycosides. However, the exception
414 to this trend was observed for the dimer with the shortest linker, Ber-C3 [**5**]), which had higher predicted
415 binding scores, primarily due increased hydrophobic interactions. Again, however, biological assays
416 corroborated these computational predictions, revealing that this ligand had increased synergy with
417 aminoglycosides and reduced the MIC to Δ*mexXY* knockout levels. Importantly, Ber-C3 [**5**] is non-toxic to
418 pseudomonal cells and appears specific for the MexXY-OprM system, unlike previously identified
419 berberine analogs[46,47] Of note, longer alkyl dimers did exhibit clear aminoglycoside-independent growth
420 inhibition, but contrary to expectation our data suggest that this phenomenon is not attributable to
421 membrane disruption. Berberine was identified to negatively impact DNA topoisomerase I/II and DNA,
422 causing cell cycle arrest and DNA damage[51-55]. In the absence of membrane effects, we therefore
423 speculate that the longer alkyl-linked berberine dimers may act similarly and studies are currently ongoing
424 to define the basis of these off-target effects.

425 Initial docking studies of berberine in the $MexY^{PAO1}$ binding pocket identified interactions with the
426 switch loop as has previously been observed[29]. Our docking of additional berberine ligands was also
427 validated through a three-way synergy assay (berberine, Ber-C3 [5], and amikacin) in PAO1 which
428 supported the predicted overlapping binding sites for these ligands. Docking analyses with berberine alkyl-
429 linked dimer analogs predicted multiple binding sites within the substrate binding region of MexY, including
430 the PBP, switch loop, DBP, and at the DBP-porter interface, highlighting the potential utility of these
431 berberine dimers as chemical probes for understanding the ligand translocation pathway and its kinetics.
432 Although binding scores for dimers with alternative aryl or PEG linkers were higher compared to the
433 comparably sized alkyl-linked dimers, these predictions were not borne out in the biological analyses for
434 these ligands. As docking analysis does not consider the process of ligand entry into MexY, we propose
435 that the dimers with more rigid and/ or hydrophobic linkers are less readily able to reach the MexY PBP/
436 DBD. Furthermore, molecular dynamics simulations suggest that possessing a short, but slightly flexible
437 linker that allows for optimal π-stacking interactions in the binding pocket is an important characteristic for
438 ligand binding to MexY.

439 Antimicrobial susceptibility testing (e.g., checkerboard assays, MICs, and time-kill assays) also
440 revealed preferential inhibition by berberine dimers for different drugs of the same class. For example, Ber-
441 pAr [**10**] showed increased synergy with gentamicin compared to other aminoglycosides tested. Further
442 development toward these specificities could thus allow berberine analogs to be used to probe specific
443 binding regions for substrates the MexXY-OprM efflux system. Additionally, reduction in MIC for non-
444 aminoglycoside substrates was possible, but inhibiting to the level of MexXY knockout in *P. aeruginosa*
445 strains was inconsistent, suggesting that these substrates can more efficiently outcompete berberine
446 analogs for binding or have alternative binding site(s), or that they are also effluxed by other RND
447 systems[56-59]. Further, we found that Ber-pAr [**10**] and Ber-C12 [**9**] had a strain-dependent effect on
448 enhanced susceptibility to non-efflux substrate imipenem, a phenomenon also previously observed in *P.*
449 *aeruginosa* PAO12 with berberine[60]. Importantly, our top berberine dimer analogs, Ber-C3 [**5**], Ber-C12 [**9**],
450 and Ber-pAr [**10**], showed promising activity against two pan-aminoglycoside resistant clinical *P.*
451 *aeruginosa* isolates with variable MexXY-OprM dependencies, K2156 and K2161, as well as *P. aeruginosa*
452 PA7 and PA14 strains. As proof-of-concept for the utility of the berberine dimers as chemical probes, we
453 were able to identify a *P. aeruginosa* strain specific residue ($MexY^{PAO1}$/ $MexY^{PA7}$ E175 *vs*. $MexY^{PA14}$ Q175)
454 which may influence inherent properties of the MexY binding pocket and therefore subsequent efflux
455 inhibition. Through checkerboard synergy assays, we identified that Ber-C3 [**5**] has reduced synergy with
456 aminoglycosides in PA14 compared to PAO1 and PA7. Docking of Ber-C3 [**5**] into all three strains MexY
457 homology models identified ligand conformational changes due to the position of the 175 residue for
458 glutamic acid versus glutamine. These data highlight the functionality of berberine dimers as probes to
459 identify putative important residues involved in MexXY-OprM efflux inhibition in multiple *P. aeruginosa*
460 strains.

461 In summary, using chemical biology and small-molecule discovery, we generated a panel of novel
462 potential probes of the transporter component of the MexXY-OprM efflux pump in *P. aeruginosa*. As RND
463 efflux pumps are ubiquitous in Gram-negative pathogens and contribute extensively to multidrug
464 resistance, understanding the chemical and mechanical properties of efflux pumps and their respective
465 substrates is imperative. Further development of chemical probes, such as our lead berberine dimers, can
466 shed light on mechanisms that govern efflux pump substrate recognition in RND efflux pumps and help
467 drive new strategies for specific EPI development.

468

469 ## Methods

470 ### Homology modeling of MexY and MexY-Per

471 The amino acid sequences of the MexY from *P. aeruginosa* PAO1, PA7 and PA14 were retrieved from
472 The *Pseudomonas* Genome Database[61] (accession codes GCF_000006765.1, GCF_000017205.1, and
473 GCF_000404265.1, respectively) and a homology model of an asymmetric MexY homotrimer was
474 constructed using the cryo-EM structure of MexB as the template (PDB 6IOL) on the Swiss Model server

475 (https://swissmodel.expasy.org). Models built with the Swiss Model server were minimized in MacroModel
476 (Schrödinger LLC 2022-3) using the OPLS4 force field and Polak-Ribier Conjugate Gradient (PRCG)
477 minimization method with 2500 iterations. A $MexY^{PAO1}$ model was also generated with the transmembrane
478 regions removed and the remaining periplasmic components joined with Gly/Ser linker ("MexY-per",
479 comprising residues: $MexY^{1-38}$-GSGSGGSGGS (linker)-$MexY^{558-863}$). The MexY-per model was
480 constructed using the full *P. aeruginosa* PAO1 MexY homology model as the starting template in Biologics
481 (Schrödinger LLC 2022-3) and with enhanced loop sampling for the linker region.
482

483 **High-throughput virtual screening (HTVS) and molecular docking**

484 The PyMol Caver plugin was used to identify potential functional pockets in the three conformationally
485 distinct protomers of the trimeric $MexY^{PAO1}$ homology model and the predicted binding pocket in the pore
486 domain of the binding conformational state protomer (chain B) was selected for HTVS and docking studies.
487 The $MexY^{PAO1}$ model from *P. aeruginosa* PAO1 was prepared for docking in Protein Preparation Wizard
488 and energy minimized prior to grid creation with OPLS4 force field (Schrodinger LLC 2022-3). For HTVS,
489 a ligand set (~10,000 berberine analogs) was created using berberine as the query in PubChem. To ensure
490 chemical diversity within this ligand set, we applied a Tanimoto coefficient cutoff of 0.8 and resultant ligands
491 were prepared in LigPrep with the OPLS4 force field (Schrödinger LLC 2022-3). A region comprising the
492 combined PBP and DBP of $MexY^{PAO1}$ was targeted using a docking grid centered between MexY residues
493 F610 and F623 with a 30 $Å^3$ outer grid (where the ligands can dock) and 15 $Å^3$ inner grid (where the ligand
494 centroid can be placed). HTVS Glide docking module (Schrödinger LLC 2022-3) was used for screening
495 of the ligand set and the top 1000 scoring ligands were re-docked with SP Glide (Schrödinger LLC 2022-
496 3). The top 100 scoring ligands from SP Glide were selected based on chemical similarity (Tanimoto
497 coefficient) using K-means clustering algorithm in the Discovery Informatics module (Schrödinger LLC
498 2022-3).

499 For additional docking studies using SP Glide, models of $MexY^{PA7}$ and $MexY^{PA14}$ were prepared as
500 for $MexY^{PAO1}$, above. Due to the flexibility of Generation 2 and Generation 3 berberine dimer linkers,
501 conventional docking could not sample all potential ligand conformations. Therefore, we used ConfGen
502 module with mixed torsional/ low mode sampling method with 100 steps/ rotatable bond and 1000 iterations
503 (Schrödinger LLC 2022-3) to generate all potential conformers of these ligands. These conformers were
504 subsequently used as the input for SP Glide docking (Schrödinger LLC 2022-3) in $MexY^{PAO1}$, $MexY^{PA7}$ and
505 $MexY^{PA14}$.
506

507 **Berberine analog synthesis**

508 *Instrumentation, chemicals, and general notes*–Nuclear magnetic resonance (NMR) spectra were
509 recorded on either a Varian INOVA 600 (600/150 MHz) or Varian INOVA 500 (500/125 MHz) spectrometer.
510 Chemical shifts are quoted in parts per million (ppm) relative to tetramethylsilane standard and with the
511 indicated solvent as an internal reference. The following abbreviations are used to describe signal

512 multiplicities: s (singlet), d (doublet), t (triplet), q (quartet), m (multiplet), br (broad), dd (doublet of doublets),
513 dt (doublet of triplets), etc. Accurate mass spectra were recorded on an Agilent 6520 Accurate-Mass Q-
514 TOF LC/MS.

515 Non-aqueous reactions were performed under an atmosphere of argon, in flame-dried glassware,
516 with HPLC-grade solvents dried by passage through activated alumina. Brine refers to a saturated aqueous
517 solution of sodium chloride, sat. $NaHCO_3$ refers to a saturated aqueous solution of sodium bicarbonate,
518 sat. NH_4Cl refers to a saturated aqueous solution of ammonium chloride, etc. "Column chromatography,"
519 unless otherwise indicated, refers to purification in a gradient of increasing ethyl acetate concentration in
520 hexanes or methanol concentration in dichloromethane on a Biotage® flash chromatography purification
521 system. All chemicals were used as received from Oakwood, TCI America, Sigma-Aldrich, Alfa Aesar, or
522 CombiBlocks.

523

524 *Experimental procedures and characterization data*–Berberrubine chloride (2.4 eq.) was combined with
525 either A. diiodide (1 eq.) or B. dibromide (1 eq.)/sodium iodide (2 eq.) in N,N-dimethylformamide (0.1 M) in
526 a sealed reaction vessel and heated to 70°C. This solution was stirred under a static argon atmosphere
527 until thin layer chromatography (TLC) analysis showed reaction completion (48-72 hours). Solvent was
528 removed *in vacuo* and product was purified via silica gel column chromatography. All synthesized analogs
529 used in biological analysis were purified to >95% purity by high-performance liquid chromatography
530 (HPLC). Additional details of all synthetic procedures and results of chemical analyses are provided in the
531 Supplementary Information.

532

533 **Bacterial strains and growth conditions**

534 Strains used in this study (**Supplemental Table S1**) were previously reported *P.* aeruginosa PAO1 (K767),
535 PAO1Δ*mexXY* (K1525), and pan-aminoglycoside resistant clinical isolates K2156 and K2161[14,19,62]. *P.*
536 *aeruginosa* PA7 and PA14 were kindly provided by Dr. Joanna Goldberg (Department of Pediatrics, Emory
537 University, Georgia, USA). Bacterial strains were maintained on Lysogeny Broth (LB)-Miller or LB-Miller
538 agar (Merck) and grown aerobically at 37°C overnight. Strains were stored in LB-Miller broth supplemented
539 with 16% glycerol at -80°C.

540

541 **DNA methods**

542 Chromosomal DNA was extracted from *P. aeruginosa* PAO1 (K767), PAO1ΔmexXY (K1525), or clinical
543 isolates K2156 and K2161 using Qiagen DNeasy Blood and Tissue Kit according to manufacturer protocol.
544 The *mexY* gene from each strain was subsequently amplified using five primers that encompass the 5'
545 and 3' ends of the gene and three internal primers to encompass all 3.1 kb. Purified PCR products were
546 sent for Sanger Sequencing (GeneWiz). Resultant FASTA sequences were aligned to *P. aeruginosa* PAO1
547 (accession GCF_000006765.1) and deposited to NCBI GenBank under the accessions OP868818 (K767),

548 OP868819 (K2156), and OP868820 (K2161). Disruption of *mexXY* in *P. aeruginosa* PAO1Δ*mexXY*
549 (K1525) was validated by colony PCR.
550
551 **Antibiotic susceptibility assays**
552 Growth conditions–For all antimicrobial susceptibility assays, *P. aeruginosa* strains were grown in cation-
553 adjusted Mueller-Hinton broth (CA-MHB) prepared using premixed MHB (Sigma) supplemented with 20
554 mg/L calcium chloride (OmniPur) and 10 mg/L magnesium chloride (Sigma). Strains were cultured
555 aerobically, shaking vigorously, at 37°C for 18 hours.
556
557 Minimum inhibitory concentration (MIC)–All MICs were determined using serial two-fold microdilution
558 method in 96-well microtiter plates as done previously[63]. Antibiotics used in this study were: kanamycin
559 (Kan; OmniPur), amikacin (Ami; ChemImpex), gentamicin (Gen; Sigma), tobramycin (Tob; Alfa Aesar),
560 cefepime (Cef; ChemImpex), ciprofloxacin (Cip; Enzo), tigecycline (Tig; Astatech), imipenem (Imi; Combi-
561 Blocks), and vancomycin (Van; Sigma). MIC values were determined at 18 hours post-inoculation by
562 reading optical density at 600 nm (OD_{600}) on a Synergy Neo2 Multi-Mode Plate Reader (Agilent BioTek),
563 and inhibition of growth defined as OD_{600}<0.5 above background. All MIC assays were performed at least
564 twice starting from fresh streak plates on separate days and each assay was performed as two technical
565 replicates. Assays were performed for all *P. aeruginosa* strains to determine starting MICs in the absence
566 of berberine or berberine analogs. All MIC assays with berberine ligands (Ber, Ber-C3 [**5**], Ber-C12 [**9**], or
567 Ber-pAr [**10**]) were adjusted for a final concentration of 1% DMSO in each well.
568
569 Checkerboard–Checkerboard assays were performed with *P. aeruginosa* PAO1 (K767) using Kan or Gen,
570 and all berberine ligands. Two-fold serial dilutions for a final concentration of Kan [256-4 µg/mL] or Gen[4-
571 0.06 µg/mL] in CA-MHB were dispensed across the rows of a 96-well microtiter plate. Berberine and
572 berberine analogs were first resuspended in 100% DMSO and then diluted with water to yield stocks [1280-
573 10 µg/mL] in 20% DMSO. Finally, the berberine and berberine analogs were dispensed down the columns
574 of the 96-well microtiter plate to give final two-fold decreasing concentrations (128-1 µg/mL) and 1% DMSO
575 final concentration. *P. aeruginosa* PAO1 (K767) was grown to OD_{600} of 0.1 in CA-MHB and was diluted to
576 a final concentration of 10^5 cells. MIC values were determined as above at 18 hours post-inoculation by
577 reading OD_{600}, where inhibition of growth defined as OD_{600}<0.5 above background. All checkerboard
578 assays were performed at least twice starting from fresh streak plates on separate days. OD_{600} readings
579 each replicate between antibiotic and berberine analog interaction were averaged and normalized from 0-
580 1.
581 For analysis of antibiotic-berberine interactions, fractional inhibitory concentration (FIC) was
582 determined as previously described[64], where a FIC value < 0.5 indicates synergy between antibiotic and
583 ligand. For berberine and berberine analogs without an experimentally measurable MIC value (i.e., greater
584 than 128 µg/mL), the final OD_{600} values from cultures at 18 hours after exposure to a range of ligand

585 concentrations (128-0 µg/mL) were plotted and nonlinear regression of the log transformed OD_{600} values
586 was used to extrapolate a calculated MIC value.
587
588 *Time-kill*–Growth curves for *P. aeruginosa* PAO1 (K767) and PAO1ΔmexXY (K1525) were measured in
589 the absence or presence of amikacin or tobramycin at concentrations ranging from ¼ to 2× the MIC and
590 with select berberine ligands (64 µg/mL). Berberine ligands were prepared and added to 96-well microtiter
591 plate as described above for the checkerboard assays. Microtiter plates containing technical replicates for
592 each antibiotic-berberine pair were incubated for 18 hours with vigorous shaking using in Cytation5
593 Imaging Reader (Agilent BioTek). OD_{600} values were recorded every 15 minutes and select time points (0,
594 2, 4, 6, 8, 10, 12, 18, and 24 hours) were plotted. Growth curves were performed in duplicate at least twice
595 from freshly streaked plates on separate days.
596
597 *Three-way synergy*–A three-way synergy assay was performed using *P. aeruginosa* PAO1 (K767) in the
598 presence of berberine (64 µg/m), Ber-C3 [**5**] (128-1 µg/mL) and Ami (4-0.06 µg/mL). The 96-well microtiter
599 plate for Ber-C3 [**5**] and amikacin was set up as a checkerboard synergy assay (as described above).
600 Berberine was added to all wells to a final concentration of 64 µg/mL and the total concentration of
601 berberine and Ber-C3 [**5**] was adjusted for a final concentration of 1% DMSO. MIC values were determined
602 as above at 18 hours post-inoculation by reading OD_{600}. The assay was performed twice using two fresh
603 streak plates for starter cultures on two different days.
604
605 **Hemolysis assay**
606 Hemolysis was performed on mechanically defibrinated sheep blood (Hemostat Labs). One mL of
607 erythrocytes was centrifuged for 10 minutes at 3,800 rpm. Supernatant was discarded, cells were washed
608 in 1 mL of 1× phosphate-buffered saline (PBS), and pelleted. This washing step was repeated five times.
609 The final pellet was diluted 20-fold in 1× PBS. Berberine and berberine ligands were resuspended in 100%
610 DMSO and the final starting concentration in each well was 2.5%. Berberine ligands were two-fold serially
611 diluted in DMSO from 128-0.5 µg/mL in a 96-well microtiter plate. 100 µL of sheep blood suspension was
612 added to 100 µL of berberine ligand, 100 µL 1% Triton-X (positive control), or 100 µL 1× PBS (negative
613 control). Samples were incubated for one hour at 37°C with shaking at 200 rpm, and then pelleted. The
614 OD_{540} of the resulting supernatant was recorded using Synergy Neo2 Multi-Mode Plate Reader (Agilent
615 BioTek). The concentration inducing 20% red blood cell lysis was calculated for each ligand based on
616 positive and negative control absorbances. Hemolysis assays were performed in triplicate.
617
618 **MD simulation and MM/GBSA calculation**
619 We used the same strategy and rationale for using a reduced model of *P. aeruginosa* PAO1 MexY-per as
620 previously described for AcrB[65,66]. The MexY-per SP Glide docking model with chemically diverse
621 berberine probes bound to the PBP and DBP binding pocket was used as a starting structure for MD

simulations. Simulations were run in duplicate with each pair of runs initiated using a different initial velocity with OPLS4 force field, producing essentially identical results. Each system was first neutralized by adding sodium ions around the protein using the System Builder module. The neutralized protein was placed in TIP3P water, and random water molecules were substituted to obtain an ionic strength of 150 mM. Each solvated system was relaxed using a series of restrained minimization stages each of 1 ns duration: 1) all heavy atoms with force constant 50 kcal/molÅ^2, all protein atoms with 2) 10 kcal/molÅ^2 and 3) 5 kcal mol kcal/molÅ^2, and finally 4) with no constraints. Unrestrained MD simulations were then performed for 60 ns, comprising 10 ns for equilibration followed by a 50 ns production run in the isothermal-isobaric (NPT) ensemble using Nose-Hoover chain thermostat and Martyna-Tobias-Klein barostat with relaxation times of 1 and 2 ps, respectively. The equations of motion were integrated using multiple time steps for short-range (2 fs) and long-range (6 fs) interactions with a 10 Å cutoff applied for non-bonded interactions. MM/GBSA calculations were performed in the Prime module (Schrödinger LLC 2022-3) with the OPLS4 force field and allowing protein side chain flexibility within a 5 Å radius of the bound ligand.

Acknowledgements

We thank Dr. Keith Poole in the Department of Biomedical and Molecular Sciences, Queens University, Ontario, Canada for providing *P. aeruginosa* PAO1, clinical isolates, and respective *mexXY* knockout strains. We thank Dr. Joanna Goldberg in the Department of Pediatrics, Emory University, Atlanta, Georgia, USA, for providing *P. aeruginosa* PA7 and PA14 isolates. This work was supported by the National Institute of General Medical Sciences (R35 GM119426 to W.M.W), National Institute of General Medical Sciences NRSA Pre-Doctoral Fellowship (F31 GM143891 to L.G.K), Cystic Fibrosis Foundation Student Traineeship (Kavana21H0 to L.G.K), an ACS MEDI Pre-doctoral Fellowship (A.R.M.), and Emory University through an Accelerator Grant from the Biological Discovery through Chemical Innovation (BDCI) initiative (to G.L.C. and W.M.W.). L.G.K. also gratefully acknowledges support from Dr. John and Linda McGowan from the Atlanta Chapter ARCS Foundation.

Author Contributions

L.G.K. and **A.R.M.** designed and performed experiments, analyzed data, and wrote the original draft and edited the manuscript; **D.D.** performed computational analyses; **W.M.W.** and **G.L.C.** conceived the study, supervised the project, and edited the manuscript. All authors jointly discussed the results and implications at all stages of the work and edited the final manuscript.

Competing Interests

The authors declare no competing interests.

Data Availability

Datasets generated during this analysis are available on NCBI GenBank under accession number BankIt2645695 OP868818-20.

References

1. Centers for Disease C, Prevention. Antibiotic Resistance Threats in the United States, 2019. Centers for Disease Control and Prevention; 2019.
2. Global burden of bacterial antimicrobial resistance in 2019: a systematic analysis. Lancet. 2022;399(10325):629-55. Epub 20220119. doi: 10.1016/s0140-6736(21)02724-0. PubMed PMID: 35065702; PMCID: PMC8841637.
3. Jurado-Martín I, Sainz-Mejías M, McClean S. Pseudomonas aeruginosa: An Audacious Pathogen with an Adaptable Arsenal of Virulence Factors. Int J Mol Sci. 2021;22(6). Epub 20210318. doi: 10.3390/ijms22063128. PubMed PMID: 33803907; PMCID: PMC8003266.
4. King J, Murphy R, Davies JC. Pseudomonas aeruginosa in the Cystic Fibrosis Lung. Adv Exp Med Biol. 2022;1386:347-69. doi: 10.1007/978-3-031-08491-1_13. PubMed PMID: 36258079.
5. Reynolds D, Kollef M. The Epidemiology and Pathogenesis and Treatment of Pseudomonas aeruginosa Infections: An Update. Drugs. 2021;81(18):2117-31. Epub 20211107. doi: 10.1007/s40265-021-01635-6. PubMed PMID: 34743315; PMCID: PMC8572145.
6. Blair JM, Richmond GE, Piddock LJ. Multidrug efflux pumps in Gram-negative bacteria and their role in antibiotic resistance. Future Microbiol. 2014;9(10):1165-77. doi: 10.2217/fmb.14.66. PubMed PMID: 25405886.
7. Kishk RM, Abdalla MO, Hashish AA, Nemr NA, El Nahhas N, Alkahtani S, Abdel-Daim MM, Kishk SM. Efflux MexAB-Mediated Resistance in P. aeruginosa Isolated from Patients with Healthcare Associated Infections. Pathogens. 2020;9(6). Epub 20200615. doi: 10.3390/pathogens9060471. PubMed PMID: 32549303; PMCID: PMC7350317.
8. Gomis-Font MA, Pitart C, Del Barrio-Tofiño E, Zboromyrska Y, Cortes-Lara S, Mulet X, Marco F, Vila J, López-Causapé C, Oliver A. Emergence of Resistance to Novel Cephalosporin-β-Lactamase Inhibitor Combinations through the Modification of the Pseudomonas aeruginosa MexCD-OprJ Efflux Pump. Antimicrob Agents Chemother. 2021;65(8):e0008921. Epub 20210716. doi: 10.1128/aac.00089-21. PubMed PMID: 34060900; PMCID: PMC8284450.
9. Xu C, Liu H, Pan X, Ma Z, Wang D, Zhang X, Zhu G, Bai F, Cheng Z, Wu W, Jin Y. Mechanisms for Development of Ciprofloxacin Resistance in a Clinical Isolate of Pseudomonas aeruginosa. Front Microbiol. 2020;11:598291. Epub 20210108. doi: 10.3389/fmicb.2020.598291. PubMed PMID: 33488544; PMCID: PMC7819972.

691 10. Singh M, Yau YCW, Wang S, Waters V, Kumar A. MexXY efflux pump overexpression and
692 aminoglycoside resistance in cystic fibrosis isolates of Pseudomonas aeruginosa from chronic
693 infections. Can J Microbiol. 2017;63(12):929-38. Epub 20170918. doi: 10.1139/cjm-2017-0380.
694 PubMed PMID: 28922614.

695 11. Davin-Regli A, Pages JM, Ferrand A. Clinical Status of Efflux Resistance Mechanisms in Gram-
696 Negative Bacteria. Antibiotics (Basel). 2021;10(9). Epub 20210916. doi:
697 10.3390/antibiotics10091117. PubMed PMID: 34572699; PMCID: PMC8467137.

698 12. Ventola CL. The Antibiotic Resistance Crisis. Pharmacy and Therapeutics. 2015;40(4):277-83.

699 13. Bhardwaj AK, Mohanty P. Bacterial efflux pumps involved in multidrug resistance and their inhibitors:
700 rejuvinating the antimicrobial chemotherapy. Recent Pat Antiinfect Drug Discov. 2012;7(1):73-89. doi:
701 10.2174/157489112799829710. PubMed PMID: 22353004.

702 14. Masuda N, Ohya S. Cross-resistance to meropenem, cephems, and quinolones in Pseudomonas
703 aeruginosa. Antimicrob Agents Chemother. 1992;36(9):1847-51. doi: 10.1128/aac.36.9.1847.
704 PubMed PMID: 1416876; PMCID: PMC192198.

705 15. Okamoto K, Gotoh N, Nishino T. Alterations of susceptibility of Pseudomonas aeruginosa by
706 overproduction of multidrug efflux systems, MexAB-OprM, MexCD-OprJ, and MexXY/OprM to
707 carbapenems: Substrate specificities of the efflux systems. Journal of Infection and Chemotherapy.
708 2002;8(4):371-3. doi: 10.1007/s10156-002-0193-7.

709 16. Morita Y, Kimura N, Mima T, Mizushima T, Tsuchiya T. Roles of MexXY- and MexAB-multidrug efflux
710 pumps in intrinsic multidrug resistance of Pseudomonas aeruginosa PAO1. J Gen Appl Microbiol.
711 2001;47(1):27-32. Epub 2002/12/17. doi: 10.2323/jgam.47.27. PubMed PMID: 12483565.

712 17. Vogne C, Aires JR, Bailly C, Hocquet D, Plésiat P. Role of the Multidrug Efflux System MexXY in the
713 Emergence of Moderate Resistance to Aminoglycosides among Pseudomonas aeruginosa Isolates
714 from Patients with Cystic Fibrosis. Antimicrobial Agents and Chemotherapy. 2004;48(5):1676-80. doi:
715 10.1128/AAC.48.5.1676-1680.2004.

716 18. Lau CH, Hughes D, Poole K. MexY-promoted aminoglycoside resistance in Pseudomonas
717 aeruginosa: involvement of a putative proximal binding pocket in aminoglycoside recognition. mBio.
718 2014;5(2):e01068. Epub 2014/04/24. doi: 10.1128/mBio.01068-14. PubMed PMID: 24757215;
719 PMCID: PMC3994515.

720 19. Sobel ML, McKay GA, Poole K. Contribution of the MexXY Multidrug Transporter to Aminoglycoside
721 Resistance in Pseudomonas aeruginosa Clinical Isolates. Antimicrobial Agents and Chemotherapy.
722 2003;47(10):3202-7. doi: 10.1128/AAC.47.10.3202-3207.2003.

723 20. Shi X, Chen M, Yu Z, Bell JM, Wang H, Forrester I, Villarreal H, Jakana J, Du D, Luisi BF, Ludtke SJ,
724 Wang Z. In situ structure and assembly of the multidrug efflux pump AcrAB-TolC. Nat Commun.

725 2019;10(1):2635. Epub 20190614. doi: 10.1038/s41467-019-10512-6. PubMed PMID: 31201302;
726 PMCID: PMC6570770.

727 21. Du D, Wang Z, James NR, Voss JE, Klimont E, Ohene-Agyei T, Venter H, Chiu W, Luisi BF.
728 Structure of the AcrAB-TolC multidrug efflux pump. Nature. 2014;509(7501):512-5. doi:
729 10.1038/nature13205.

730 22. Tsutsumi K, Yonehara R, Ishizaka-Ikeda E, Miyazaki N, Maeda S, Iwasaki K, Nakagawa A,
731 Yamashita E. Structures of the wild-type MexAB–OprM tripartite pump reveal its complex formation
732 and drug efflux mechanism. Nature Communications. 2019;10(1):1520. doi: 10.1038/s41467-019-
733 09463-9.

734 23. Nakashima R, Sakurai K, Yamasaki S, Hayashi K, Nagata C, Hoshino K, Onodera Y, Nishino K,
735 Yamaguchi A. Structural basis for the inhibition of bacterial multidrug exporters. Nature.
736 2013;500(7460):102-6. doi: 10.1038/nature12300.

737 24. Murakami S, Nakashima R, Yamashita E, Matsumoto T, Yamaguchi A. Crystal structures of a
738 multidrug transporter reveal a functionally rotating mechanism. Nature. 2006;443(7108):173-9. doi:
739 10.1038/nature05076.

740 25. Seeger MA, Schiefner A, Eicher T, Verrey F, Diederichs K, Pos KM. Structural asymmetry of AcrB
741 trimer suggests a peristaltic pump mechanism. Science. 2006;313(5791):1295-8. doi:
742 10.1126/science.1131542. PubMed PMID: 16946072.

743 26. Sennhauser G, Amstutz P, Briand C, Storchenegger O, Grütter MG. Drug Export Pathway of
744 Multidrug Exporter AcrB Revealed by DARPin Inhibitors. PLoS Biology. 2007;5(1). doi:
745 10.1371/journal.pbio.0050007.

746 27. Seeger MA, Diederichs K, Eicher T, Brandstätter L, Schiefner A, Verrey F, Pos KM. The AcrB efflux
747 pump: conformational cycling and peristalsis lead to multidrug resistance. Curr Drug Targets.
748 2008;9(9):729-49. doi: 10.2174/138945008785747789. PubMed PMID: 18781920.

749 28. Müller RT, Travers T, Cha HJ, Phillips JL, Gnanakaran S, Pos KM. Switch Loop Flexibility Affects
750 Substrate Transport of the AcrB Efflux Pump. J Mol Biol. 2017;429(24):3863-74. Epub 20171005.
751 doi: 10.1016/j.jmb.2017.09.018. PubMed PMID: 28987732.

752 29. Laudadio E, Cedraro N, Mangiaterra G, Citterio B, Mobbili G, Minnelli C, Bizzaro D, Biavasco F,
753 Galeazzi R. Natural Alkaloid Berberine Activity against Pseudomonas aeruginosa MexXY-Mediated
754 Aminoglycoside Resistance: In Silico and in Vitro Studies. J Nat Prod. 2019;82(7):1935-44. Epub
755 20190705. doi: 10.1021/acs.jnatprod.9b00317. PubMed PMID: 31274312.

756 30. Morita Y, Nakashima K, Nishino K, Kotani K, Tomida J, Inoue M, Kawamura Y. Berberine Is a Novel
757 Type Efflux Inhibitor Which Attenuates the MexXY-Mediated Aminoglycoside Resistance in

758 Pseudomonas aeruginosa. Front Microbiol. 2016;7:1223. Epub 2016/08/23. doi:
759 10.3389/fmicb.2016.01223. PubMed PMID: 27547203; PMCID: PMC4975076.

760 31. Dey D, Kavanaugh LG, Conn GL. Antibiotic Substrate Selectivity of MexY and MexB Efflux Systems
761 Is Determined by a Goldilocks Affinity. Antimicrobial Agents and Chemotherapy. 2020;64(8):e00496-
762 20, /aac/64/8/AAC.-20.atom. doi: 10.1128/AAC.00496-20.

763 32. Jennings MC, Ator LE, Paniak TJ, Minbiole KP, Wuest WM. Biofilm-eradicating properties of
764 quaternary ammonium amphiphiles: simple mimics of antimicrobial peptides. Chembiochem.
765 2014;15(15):2211-5. Epub 20140821. doi: 10.1002/cbic.201402254. PubMed PMID: 25147134.

766 33. Alkhalifa S, Jennings MC, Granata D, Klein M, Wuest WM, Minbiole KPC, Carnevale V. Analysis of
767 the Destabilization of Bacterial Membranes by Quaternary Ammonium Compounds: A Combined
768 Experimental and Computational Study. Chembiochem. 2020;21(10):1510-6. Epub 20200218. doi:
769 10.1002/cbic.201900698. PubMed PMID: 31859426; PMCID: PMC7237276.

770 34. Muheim C, Götzke H, Eriksson AU, Lindberg S, Lauritsen I, Nørholm MHH, Daley DO. Increasing the
771 permeability of Escherichia coli using MAC13243. Sci Rep. 2017;7(1):17629. Epub 20171215. doi:
772 10.1038/s41598-017-17772-6. PubMed PMID: 29247166; PMCID: PMC5732295.

773 35. Sobel ML, McKay GA, Poole K. Contribution of the MexXY multidrug transporter to aminoglycoside
774 resistance in Pseudomonas aeruginosa clinical isolates. Antimicrob Agents Chemother.
775 2003;47(10):3202-7. Epub 2003/09/25. doi: 10.1128/aac.47.10.3202-3207.2003. PubMed PMID:
776 14506031; PMCID: PMC201159.

777 36. Lomovskaya O, Bostian KA. Practical applications and feasibility of efflux pump inhibitors in the
778 clinic—A vision for applied use. Biochemical Pharmacology. 2006;71(7):910-8. doi:
779 https://doi.org/10.1016/j.bcp.2005.12.008.

780 37. Mesaros N, Glupczynski Y, Avrain L, Caceres NE, Tulkens PM, Van Bambeke F. A combined
781 phenotypic and genotypic method for the detection of Mex efflux pumps in Pseudomonas
782 aeruginosa. J Antimicrob Chemother. 2007;59(3):378-86. Epub 2007/02/10. doi: 10.1093/jac/dkl504.
783 PubMed PMID: 17289770.

784 38. Bhattacharyya T, Sharma A, Akhter J, Pathania R. The small molecule IITR08027 restores the
785 antibacterial activity of fluoroquinolones against multidrug-resistant Acinetobacter baumannii by efflux
786 inhibition. Int J Antimicrob Agents. 2017;50(2):219-26. Epub 2017/05/24. doi:
787 10.1016/j.ijantimicag.2017.03.005. PubMed PMID: 28533185.

788 39. Osei Sekyere J, Amoako DG. Carbonyl Cyanide m-Chlorophenylhydrazine (CCCP) Reverses
789 Resistance to Colistin, but Not to Carbapenems and Tigecycline in Multidrug-Resistant
790 Enterobacteriaceae. Front Microbiol. 2017;8:228. Epub 2017/03/07. doi: 10.3389/fmicb.2017.00228.
791 PubMed PMID: 28261184; PMCID: PMC5306282.

792 40. Whalen KE, Poulson-Ellestad KL, Deering RW, Rowley DC, Mincer TJ. Enhancement of antibiotic
793 activity against multidrug-resistant bacteria by the efflux pump inhibitor 3,4-dibromopyrrole-2,5-dione
794 isolated from a Pseudoalteromonas sp. J Nat Prod. 2015;78(3):402-12. Epub 2015/02/04. doi:
795 10.1021/np500775e. PubMed PMID: 25646964.

796 41. Li XZ, Plésiat P, Nikaido H. The challenge of efflux-mediated antibiotic resistance in Gram-negative
797 bacteria. Clin Microbiol Rev. 2015;28(2):337-418. doi: 10.1128/cmr.00117-14. PubMed PMID:
798 25788514; PMCID: PMC4402952.

799 42. Imanshahidi M, Hosseinzadeh H. Pharmacological and therapeutic effects of Berberis vulgaris and its
800 active constituent, berberine. Phytother Res. 2008;22(8):999-1012. doi: 10.1002/ptr.2399. PubMed
801 PMID: 18618524.

802 43. Kulkarni SK, Dhir A. Berberine: a plant alkaloid with therapeutic potential for central nervous system
803 disorders. Phytother Res. 2010;24(3):317-24. doi: 10.1002/ptr.2968. PubMed PMID: 19998323.

804 44. Vuddanda PR, Chakraborty S, Singh S. Berberine: a potential phytochemical with multispectrum
805 therapeutic activities. Expert Opin Investig Drugs. 2010;19(10):1297-307. doi:
806 10.1517/13543784.2010.517745. PubMed PMID: 20836620.

807 45. Liang Y, Xu X, Yin M, Zhang Y, Huang L, Chen R, Ni J. Effects of berberine on blood glucose in
808 patients with type 2 diabetes mellitus: a systematic literature review and a meta-analysis. Endocr J.
809 2019;66(1):51-63. Epub 20181103. doi: 10.1507/endocrj.EJ18-0109. PubMed PMID: 30393248.

810 46. Giorgini G, Mangiaterra G, Cedraro N, Laudadio E, Sabbatini G, Cantarini M, Minnelli C, Mobbili G,
811 Frangipani E, Biavasco F, Galeazzi R. Berberine Derivatives as Pseudomonas aeruginosa MexXY-
812 OprM Inhibitors: Activity and In Silico Insights. Molecules. 2021;26(21). Epub 20211102. doi:
813 10.3390/molecules26216644. PubMed PMID: 34771051; PMCID: PMC8587913.

814 47. Kotani K, Matsumura M, Morita Y, Tomida J, Kutsuna R, Nishino K, Yasuike S, Kawamura Y. 13-(2-
815 Methylbenzyl) Berberine Is a More Potent Inhibitor of MexXY-Dependent Aminoglycoside Resistance
816 than Berberine. Antibiotics (Basel). 2019;8(4). Epub 2019/11/09. doi: 10.3390/antibiotics8040212.
817 PubMed PMID: 31698691; PMCID: PMC6963850.

818 48. Plé C, Tam HK, Vieira Da Cruz A, Compagne N, Jiménez-Castellanos JC, Müller RT, Pradel E,
819 Foong WE, Malloci G, Ballée A, Kirchner MA, Moshfegh P, Herledan A, Herrmann A, Deprez B,
820 Willand N, Vargiu AV, Pos KM, Flipo M, Hartkoorn RC. Pyridylpiperazine-based allosteric inhibitors of
821 RND-type multidrug efflux pumps. Nat Commun. 2022;13(1):115. Epub 20220110. doi:
822 10.1038/s41467-021-27726-2. PubMed PMID: 35013254; PMCID: PMC8749003.

823 49. Giri P, Kumar GS. Isoquinoline alkaloids and their binding with polyadenylic acid: potential basis of
824 therapeutic action. Mini Rev Med Chem. 2010;10(7):568-77. doi: 10.2174/138955710791384009.
825 PubMed PMID: 20500148.

826 50. Tera M, Hirokawa T, Okabe S, Sugahara K, Seimiya H, Shimamoto K. Design and synthesis of a
827 berberine dimer: a fluorescent ligand with high affinity towards G-quadruplexes. Chemistry.
828 2015;21(41):14519-28. Epub 20150813. doi: 10.1002/chem.201501693. PubMed PMID: 26272465.

829 51. Krishnan P, Bastow KF. The 9-position in berberine analogs is an important determinant of DNA
830 topoisomerase II inhibition. Anticancer Drug Des. 2000;15(4):255-64. PubMed PMID: 11200501.

831 52. Qin Y, Pang JY, Chen WH, Zhao ZZ, Liu L, Jiang ZH. Inhibition of DNA topoisomerase I by natural
832 and synthetic mono- and dimeric protoberberine alkaloids. Chem Biodivers. 2007;4(3):481-7. doi:
833 10.1002/cbdv.200790040. PubMed PMID: 17372950.

834 53. Kim JB, Yu JH, Ko E, Lee KW, Song AK, Park SY, Shin I, Han W, Noh DY. The alkaloid Berberine
835 inhibits the growth of Anoikis-resistant MCF-7 and MDA-MB-231 breast cancer cell lines by inducing
836 cell cycle arrest. Phytomedicine. 2010;17(6):436-40. Epub 20091002. doi:
837 10.1016/j.phymed.2009.08.012. PubMed PMID: 19800775.

838 54. Li DD, Xu Y, Zhang DZ, Quan H, Mylonakis E, Hu DD, Li MB, Zhao LX, Zhu LH, Wang Y, Jiang YY.
839 Fluconazole assists berberine to kill fluconazole-resistant Candida albicans. Antimicrob Agents
840 Chemother. 2013;57(12):6016-27. Epub 20130923. doi: 10.1128/aac.00499-13. PubMed PMID:
841 24060867; PMCID: PMC3837902.

842 55. Domadia PN, Bhunia A, Sivaraman J, Swarup S, Dasgupta D. Berberine targets assembly of
843 Escherichia coli cell division protein FtsZ. Biochemistry. 2008;47(10):3225-34. Epub 20080215. doi:
844 10.1021/bi7018546. PubMed PMID: 18275156.

845 56. Dean CR, Visalli MA, Projan SJ, Sum PE, Bradford PA. Efflux-mediated resistance to tigecycline
846 (GAR-936) in Pseudomonas aeruginosa PAO1. Antimicrob Agents Chemother. 2003;47(3):972-8.
847 doi: 10.1128/aac.47.3.972-978.2003. PubMed PMID: 12604529; PMCID: PMC149306.

848 57. Jeannot K, Elsen S, Köhler T, Attree I, van Delden C, Plésiat P. Resistance and virulence of
849 Pseudomonas aeruginosa clinical strains overproducing the MexCD-OprJ efflux pump. Antimicrob
850 Agents Chemother. 2008;52(7):2455-62. Epub 20080512. doi: 10.1128/aac.01107-07. PubMed
851 PMID: 18474583; PMCID: PMC2443911.

852 58. Zhao L, Wang S, Li X, He X, Jian L. Development of in vitro resistance to fluoroquinolones in
853 Pseudomonas aeruginosa. Antimicrob Resist Infect Control. 2020;9(1):124. Epub 20200805. doi:
854 10.1186/s13756-020-00793-8. PubMed PMID: 32758289; PMCID: PMC7405379.

855 59. Lee A, Mao W, Warren MS, Mistry A, Hoshino K, Okumura R, Ishida H, Lomovskaya O. Interplay
856 between efflux pumps may provide either additive or multiplicative effects on drug resistance. J
857 Bacteriol. 2000;182(11):3142-50. doi: 10.1128/jb.182.11.3142-3150.2000. PubMed PMID: 10809693;
858 PMCID: PMC94500.

859 60. Su F, Wang J. Berberine inhibits the MexXY-OprM efflux pump to reverse imipenem resistance in a
860 clinical carbapenem-resistant Pseudomonas aeruginosa isolate in a planktonic state. Exp Ther Med.
861 2018;15(1):467-72. Epub 20171101. doi: 10.3892/etm.2017.5431. PubMed PMID: 29387199;
862 PMCID: PMC5769289.

863 61. Winsor GL, Griffiths EJ, Lo R, Dhillon BK, Shay JA, Brinkman FS. Enhanced annotations and
864 features for comparing thousands of Pseudomonas genomes in the Pseudomonas genome
865 database. Nucleic Acids Res. 2016;44(D1):D646-53. Epub 20151117. doi: 10.1093/nar/gkv1227.
866 PubMed PMID: 26578582; PMCID: PMC4702867.

867 62. De Kievit TR, Parkins MD, Gillis RJ, Srikumar R, Ceri H, Poole K, Iglewski BH, Storey DG. Multidrug
868 efflux pumps: expression patterns and contribution to antibiotic resistance in Pseudomonas
869 aeruginosa biofilms. Antimicrob Agents Chemother. 2001;45(6):1761-70. doi:
870 10.1128/aac.45.6.1761-1770.2001. PubMed PMID: 11353623; PMCID: PMC90543.

871 63. Wiegand I, Hilpert K, Hancock RE. Agar and broth dilution methods to determine the minimal
872 inhibitory concentration (MIC) of antimicrobial substances. Nat Protoc. 2008;3(2):163-75. doi:
873 10.1038/nprot.2007.521. PubMed PMID: 18274517.

874 64. Meletiadis J, Pournaras S, Roilides E, Walsh TJ. Defining fractional inhibitory concentration index
875 cutoffs for additive interactions based on self-drug additive combinations, Monte Carlo simulation
876 analysis, and in vitro-in vivo correlation data for antifungal drug combinations against Aspergillus
877 fumigatus. Antimicrob Agents Chemother. 2010;54(2):602-9. Epub 20091207. doi:
878 10.1128/aac.00999-09. PubMed PMID: 19995928; PMCID: PMC2812160.

879 65. Ruggerone P, Vargiu AV, Collu F, Fischer N, Kandt C. Molecular Dynamics Computer Simulations of
880 Multidrug RND Efflux Pumps. Comput Struct Biotechnol J. 2013;5:e201302008. Epub 20130303. doi:
881 10.5936/csbj.201302008. PubMed PMID: 24688701; PMCID: PMC3962194.

882 66. Vargiu AV, Nikaido H. Multidrug binding properties of the AcrB efflux pump characterized by
883 molecular dynamics simulations. Proc Natl Acad Sci U S A. 2012;109(50):20637-42. Epub 20121121.
884 doi: 10.1073/pnas.1218348109. PubMed PMID: 23175790; PMCID: PMC3528587.

885

Tables

Table 1. Aminoglycoside minimum inhibitory concentration (MIC) against *P. aeruginosa* PAO1 in the presence of berberine and berberine analogs (64 µg/mL).

Strain	Berberine analog	MIC; µg/mL[a] (fold change)[b]			
		Kan	Gen	Ami	Tob
PAO1	-	64	1	1	0.5
PAO1Δ*mexXY*	-	16 (4)	0.25 (4)	0.25 (4)	0.25 (2)
PAO1	Berberine	32 (2)	0.5 (2)	0.5 (2)	0.25 (2)
	Ber-Pip [**1**]	64 (-)	1 (-)	*nd*	*nd*
	Ber-Carb [**2**]	32 (2)	0.5 (2)	*nd*	*nd*
	Ber-Prop [**3**]	32 (2)	0.5 (2)	*nd*	*nd*
	Ber-C3 [**5**]	16 (4)	0.25 (4)	0.25 (4)	0.25 (2)
	Ber-C4 [**6**]	16 (4)	0.25 (4)	0.5 (2)	0.25 (2)
	Ber-C6 [**4**]	16 (4)	0.25 (4)	*nd*	*nd*
	Ber-C8 [**7**]	16 (4)	0.125 (6)	*nd*	*nd*
	Ber-C10 [**8**]	8 (6)	0.0625 (8)	0.0125 (6)	0.0625 (6)
	Ber-C12 [**9**]	8 (6)	0.125 (6)	0.125 (6)	0.125 (4)
	Ber-pAr [**10**]	32 (2)	0.25 (4)	0.5 (2)	0.25 (2)
	Ber-Biph [**11**]	32 (2)	0.5 (2)	*nd*	*nd*
	Ber-PEG5 [**12**]	32 (2)	0.5 (2)	0.5 (2)	0.25 (2)
	Ber-PEG8 [**13**]	32 (2)	0.5 (2)	0.5 (2)	0.25 (2)

[a]Determined from checkerboard and time-kill assays. Aminoglycosides: kanamycin (Kan), amikacin (Ami), gentamicin (Gen), and tobramycin (Tob); *nd*, not determined.

[b]fold change relative to wild-type PAO1. (-)no fold change.

Table 2. Gentamicin MIC against *P. aeruginosa* strains PA7 and PA14 in the absence and presence of berberine or select analogs.

Strain	Gentamicin MIC, µg/mL (fold change)[a,b,c]				
	-	Berberine	Ber-C3 [**5**]	Ber-C12 [**9**]	Ber-pAr [**10**]
PAO1	1	0.5 (2)	0.25 (4)	0.125 (8)	0.25 (4)
PA7	256	128/64 (2/4)	32 (6)	32 (6)	64 (4)
PA14	2	2/1 (-/2)	1 (2)	1 (2)	2/1 (-/2)

[a]Berberine or analog included at 64 µg/mL.
[b]MIC data for PAO1 are the same as in Table S4 and are shown for ease of comparison.
[c]fold change is relative to respective to wild-type PAO1, PA7, or PA14, (-) represents no fold change

Table 3. Antibiotic minimum inhibitory concentration (MIC) in absence or presence of select berberine analogs for *P. aeruginosa* PAO1 and two clinical pan-aminoglycoside resistant strains (K2156 and K2161).

	Antibiotic MIC;µg/mL[c] (fold change)[d]					
Genotype	WT	ΔXY[b]	WT			
Analog[a]	-	-	Berberine	Ber-C3 [**5**]	Ber C12 [**9**]	Ber-pAr [**10**]
P. aeruginosa PAO1						
Kan	64	16 (4)	32 (2)	16 (4)	8 (6)	32 (2)
Ami	1	0.25 (4)	0.5 (2)	0.25 (4)	0.125 (6)	0.5 (2)
Gen	1	0.25 (4)	0.5 (2)	0.25 (4)	0.125 (6)	0.25 (4)
Tob	0.5	0.25 (2)	0.25 (2)	0.25 (2)	0.125 (4)	0.25 (2)
Tig	4	0.5 (6)	4 (-)	2 (2)	2 (2)	4 (-)
Cef	1	0.5 (2)	1 (-)	0.5 (2)	2 (+2)	1 (-)
Cip	0.125	0.125 (-)	0.125 (-)	0.125 (-)	0.5 (+4)	0.25 (+2)
Imi	4	4 (-)	4 (-)	4 (-)	2 (2)	2 (2)
Pan-aminoglycoside resistant *P. aeruginosa* clinical isolate K2156						
Kan	256	16 (8)	16 (8)	16 (8)	8 (10)	16 (8)
Ami	8	0.5 (8)	0.5 (8)	0.5 (8)	0.5 (8)	0.5 (8)
Gen	8	0.5 (8)	1 (6)	0.5 (8)	0.5 (8)	1 (6)
Tob	2	1 (2)	0.5 (4)	0.25 (6)	0.5 (4)	0.5 (4)
Tig	4	0.5 (6)	4 (-)	2 (2)	1 (4)	4 (-)
Cef	2	1 (2)	2 (-)	2 (-)	2 (-)	2 (-)
Cip	1	1 (-)	1 (-)	1 (-)	4 (+4)	2 (+2)
Imi	2 (-)	2 (-)	2 (-)	2 (-)	2 (-)	2 (-)
Pan-aminoglycoside resistant *P. aeruginosa* clinical isolate K2161						
Kan	256	64 (4)	256 (-)	128 (2)	128 (2)	256 (-)
Ami	16	2 (6)	8 (2)	4 (4)	8 (2)	8 (2)
Gen	16	2 (6)	8 (2)	4 (4)	4 (4)	8 (2)
Tob	8	2 (4)	4 (2)	2 (4)	2 (4)	4 (2)
Tig	4	1 (4)	4 (-)	4 (-)	2 (2)	4 (-)
Cef	0.25	0.125 (2)	0.5 (+2)	0.25 (-)	1 (+4)	1 (+4)
Cip	0.125	0.06 (2)	0.25 (+2)	0.25 (+2)	0.5 (+4)	0.25 (+2)
Imi	2	2 (-)	2 (-)	2 (-)	1 (2)	2 (-)

[a]Berberine or dimeric analog included at a fixed concentration of 64 µg/mL where indicated.
[b]Isogenic MexXY knockout of the corresponding parental strain, PAO1 or clinical isolate.
[c]Antibiotics include MexXY-OprM substrates kanamycin (Kan), amikacin (Ami), gentamicin (Gen), tobramycin (Tob), tigecycline (Tig), cefepime (Cef), and ciprofloxacin (Cip), and the nonsubstrate imipenem (Imi).
[d]fold decrease relative to respective wild type PAO1, K2156, or K2161. (-) indicates no change. (+) indicates an increase in MIC.

Schemes

Scheme 1. Overview of berberine analog synthesis.

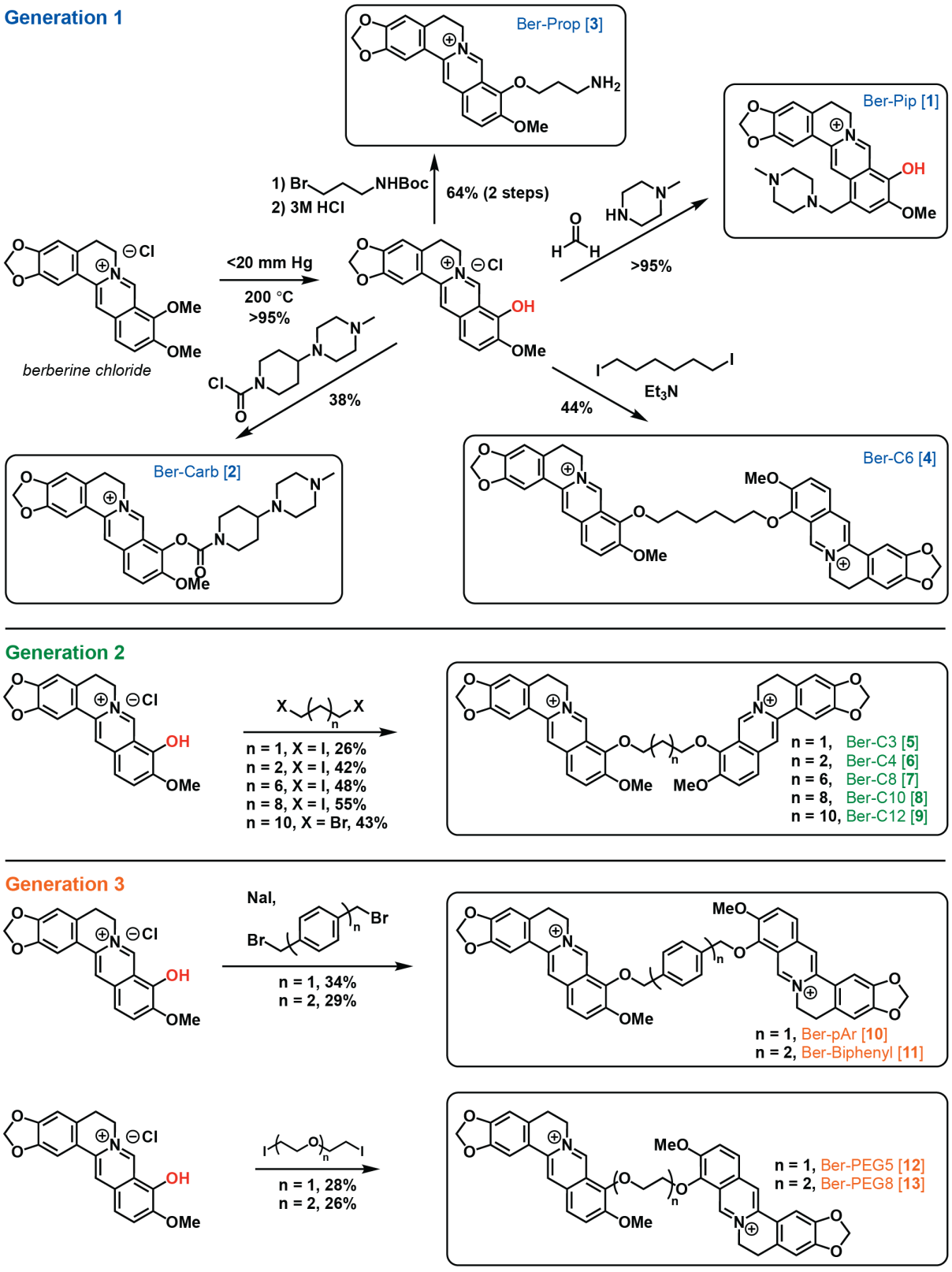

Figures and Legends

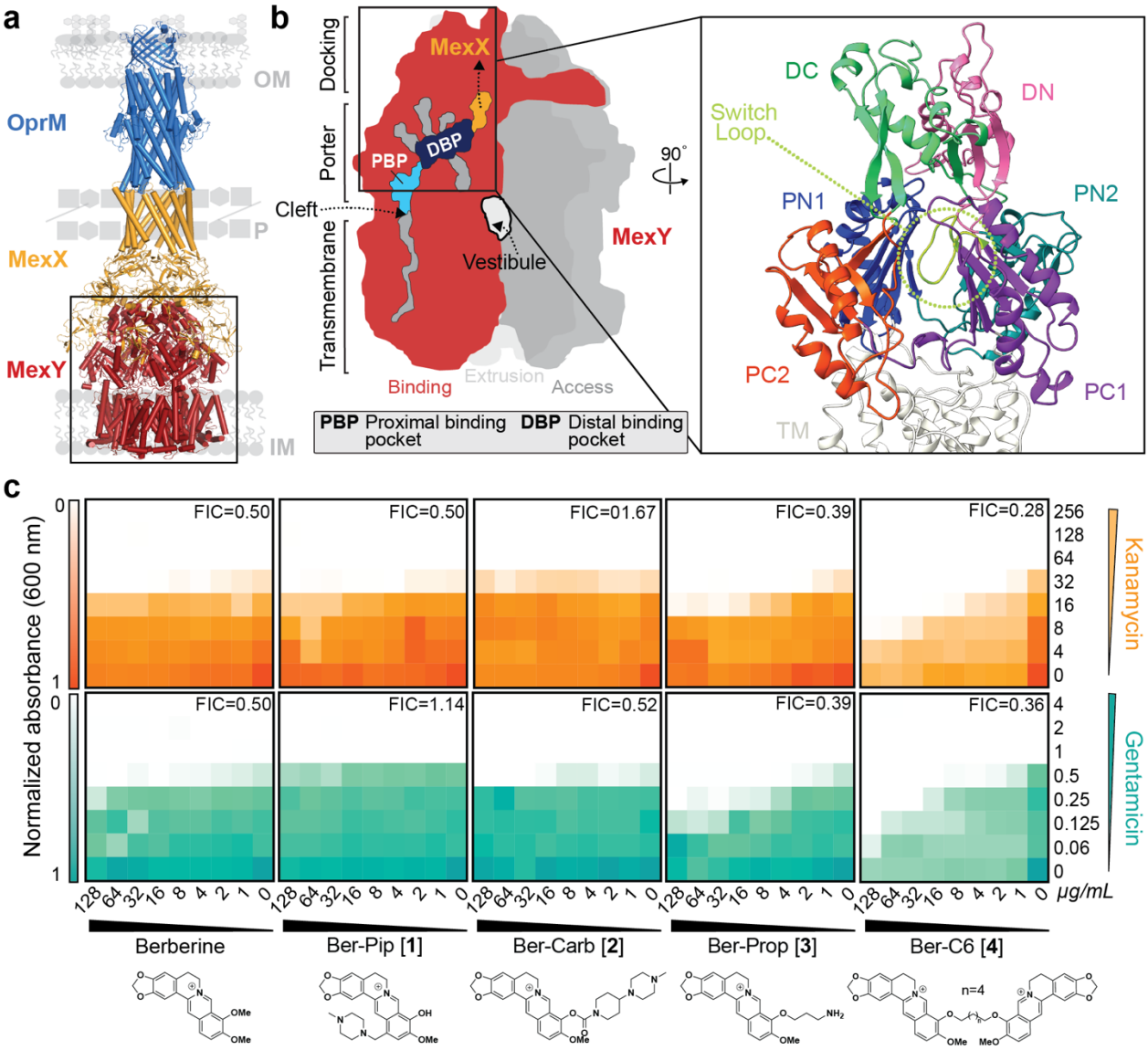

Fig. 1. HTVS identifies berberine analogs as potential probes of MexY. (**a**) Homology model of the MexXY-OprM RND system comprising outer membrane (OM) protein OprM (blue), periplasmic (P) adaptor protein MexX (gold), and inner membrane (IM) transporter MexY (red). (**b**) Schematic of the MexY homotrimer in its three conformational states: access (dark grey), binding (red), and extrusion (light grey). The two putative main substrate entry channels (cleft and vestibule), primary substrate binding region (DBP and PBP), and path to MexX are indicated. A zoomed in view of the binding pocket structure (boxed) also highlights the MexX docking domain, DC (light green) and DN (pink), the porter domain, PN1 (blue), PN2 (teal), PC1 (purple), PC2 (orange), and the switch loop (lime green). (**c**) Checkerboard synergy assays in *P. aeruginosa* PAO1 with berberine and selected analogs from HTVS (*Generation 1*). Increased synergy is observed for Ber-Prop [**3**] and Ber-C6 [**4**] with Kan (top, orange) and Gen (bottom, teal) compared to berberine. Data are shown as the normalized mean of the optical density (OD_{600}) of two biological replicates (0 is no growth, and 1 is maximum growth). The lowest Fractional Inhibitory Concentration (FIC) score for each compound-antibiotic pair is given in the upper right corner.

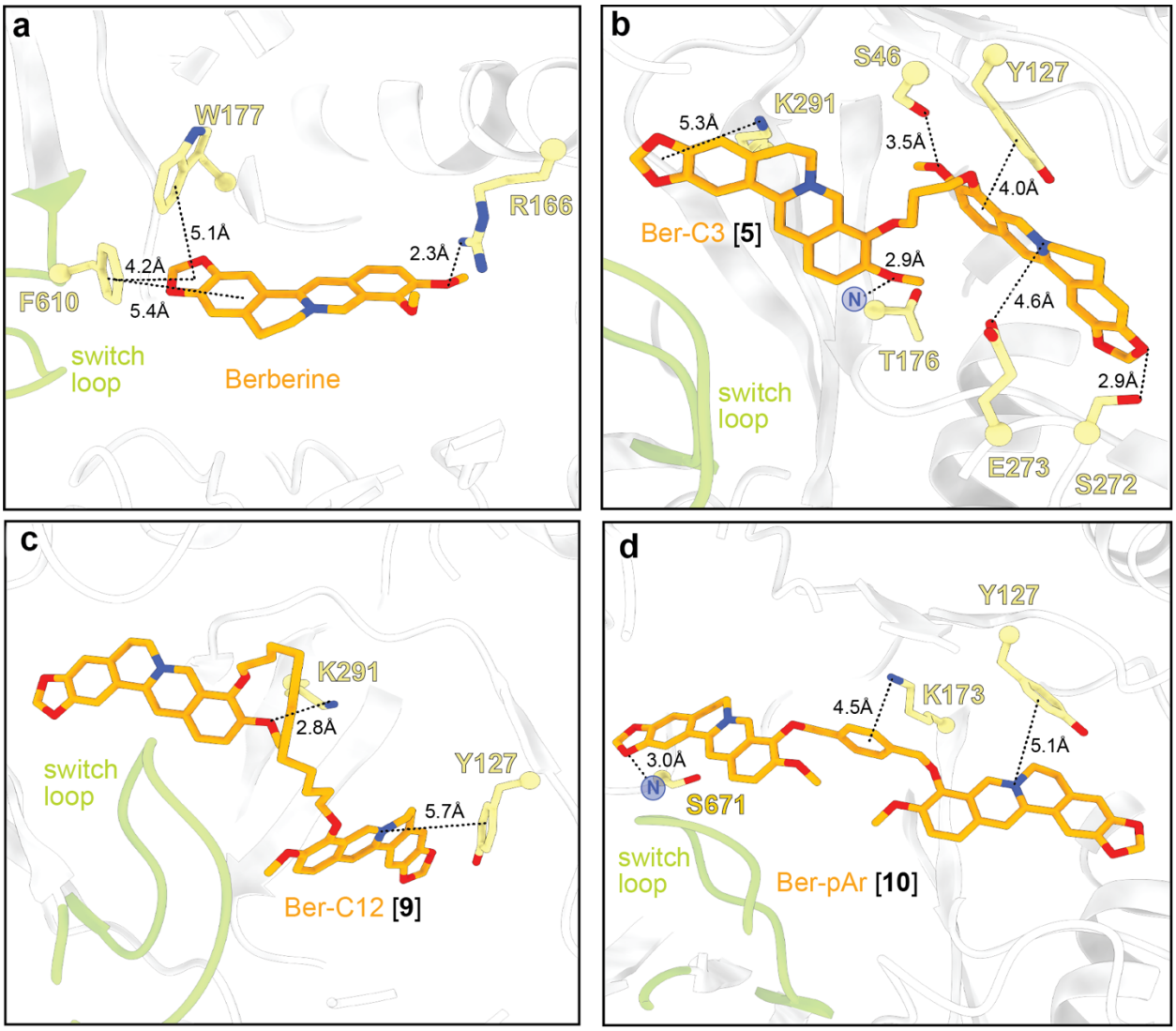

Fig. 2. Predicted docking of select berberine analogs in the MexY^{PAO1} binding pocket reveals potential ligand-specific interactions. Docking of **(a)** berberine and the top three ligands of interest **(b)** Ber-C3 [**5**] , **(c)** Ber-C12 [**9**], and **(d)** Ber-pAr [**10**] in the MexY^{PAO1} binding pocket spanning from the PBP to the DBP. Berberine docks in the DBP at the switch loop, Ber-C3 [**5**] and Ber-C12 [**9**] show preference for docking in the DBP, and Ber-pAr [**10**] spans the PBP and DBP.

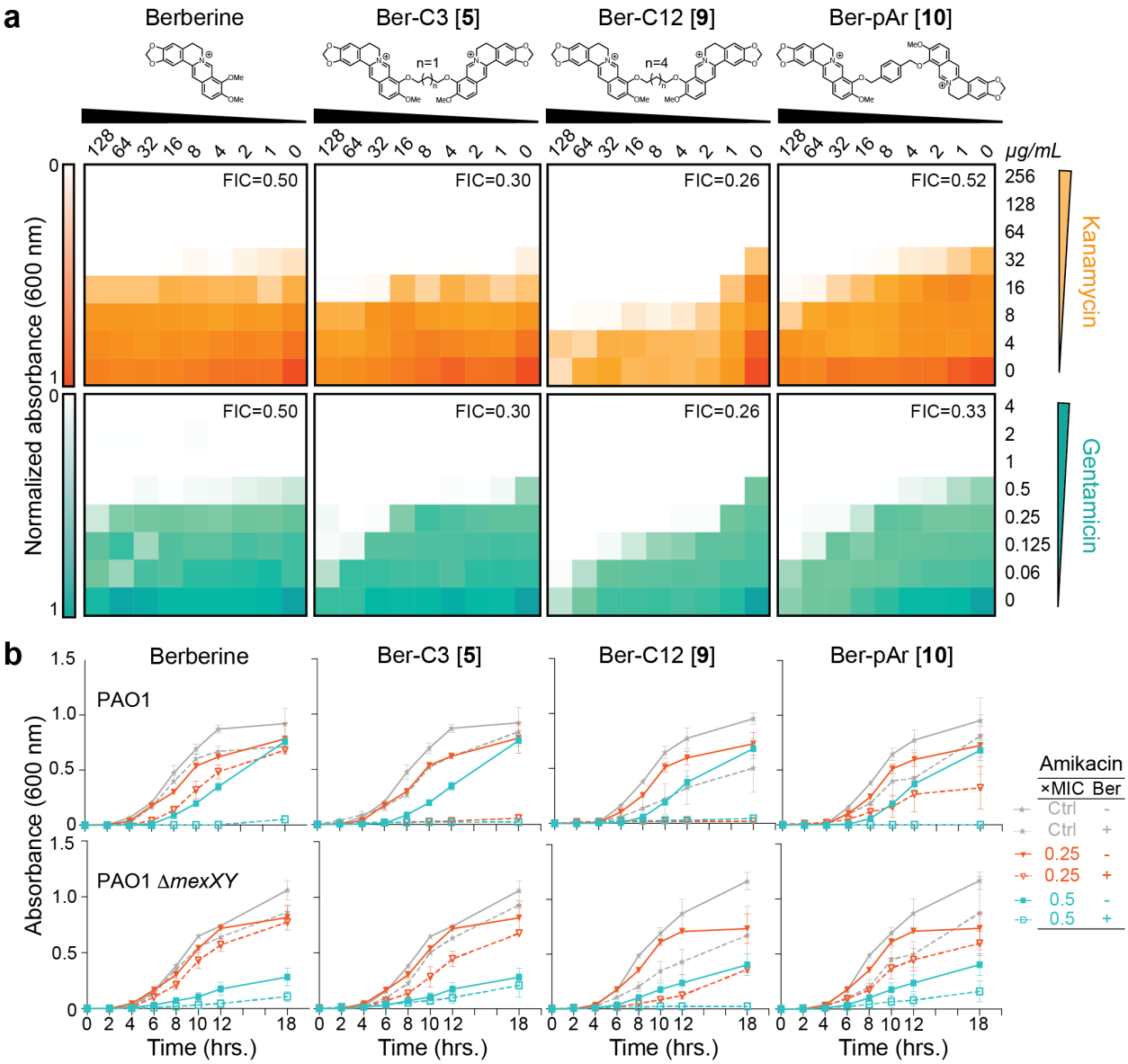

Fig. 3. Top berberine dimers exhibit increased synergy with aminoglycosides compared to berberine. (a) Checkerboard synergy assays with berberine and top selected berberine dimers in *P. aeruginosa* PAO1. Increased synergy is observed with all ligands and kanamycin (top, orange) and gentamicin (bottom, teal) compared to natural berberine. The lowest fractional inhibitory concentration (FIC) score obtained is shown in the top right corner of each plot. Data are shown as the normalized mean of the optical density (OD_{600}) of two biological replicates (0 is no growth, and 1 is maximum growth). **(b)** Time-kill assays for berberine and dimer analogs at 64 μg/mL performed over 18 hours in both *P. aeruginosa* PAO1 (top) and its *mexXY* isogenic knockout (bottom). Synergy was observed with amikacin for all ligands tested, and Ber-C3 and Ber-C12 reduced the MIC four-fold (red open triangle) compared to no berberine dimer (red filled triangle). Berberine and Ber-pAr reduce the MIC by only two-fold (teal open square) at the tested concentration compared to no berberine dimer (teal filled square). Significant aminoglycoside-independent growth inhibition is observed for Ber-C12 (dashed grey line) compared to the no antibiotic growth control (grey line). Two-fold reduction of the MIC (black open square) for Ber-C12 in *P. aeruginosa* PAO1Δ*mexXY* also suggests off-target activity. Data are shown as the average OD_{600} of biological replicates, each with two technical replicates, with error bars representing the standard deviation.

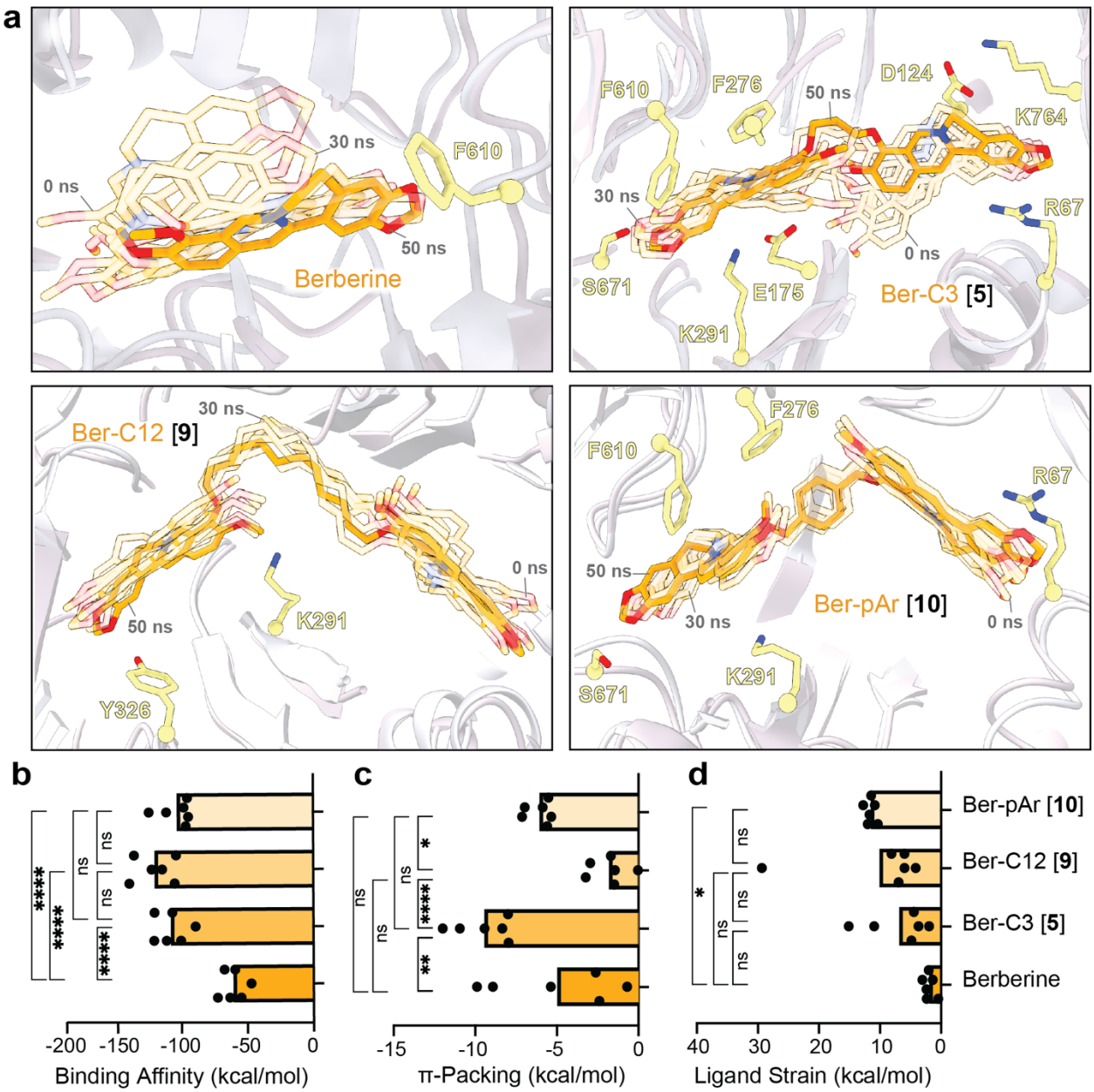

Fig. 4. Molecular dynamics simulations of berberine and berberine dimers reveal important characteristics for effective chemical probes of efflux function by MexY. (a) 50 ns molecular dynamics simulations of berberine (top left) and berberine dimers, Ber-C3 [**5**] (top right), and Ber-C12 [**9**] (bottom left), and Ber-pAr [**10**] (bottom right) in the MexY^{PAO1} DBP and PBP. Conformations at the start (0 ns) and every 10 ns are shown as semi-transparent sticks (0 and 30 ns frames are indicated) and the final conformation (at 50 ns) is shown as solid sticks (orange). Parameters derived from MM/GBSA calculations: **(b)** binding affinity, **(c)** π-packing, and **(d)** ligand strain. Data shown are the individual calculated values for six frames (0 ns and one per 10 ns segment between 0-50 ns) with the average shown as a bar plot. Ber-C3 [**5**] was found to be an effective and specific efflux pump inhibitor for the MexXY-OprM efflux system compared to berberine, Ber-pAr [**9**] and Ber-C12 [**10**]. Statistical analysis was performed using one-way ANOVA on the mean for each ligand and a post-hoc Turkey test was used for pairwise comparison. Statistically significant results are shown (* $p \leq 0.05$, ** $p \leq 0.01$, *** $p \leq 0.001$, and **** $p \leq 0.0001$).

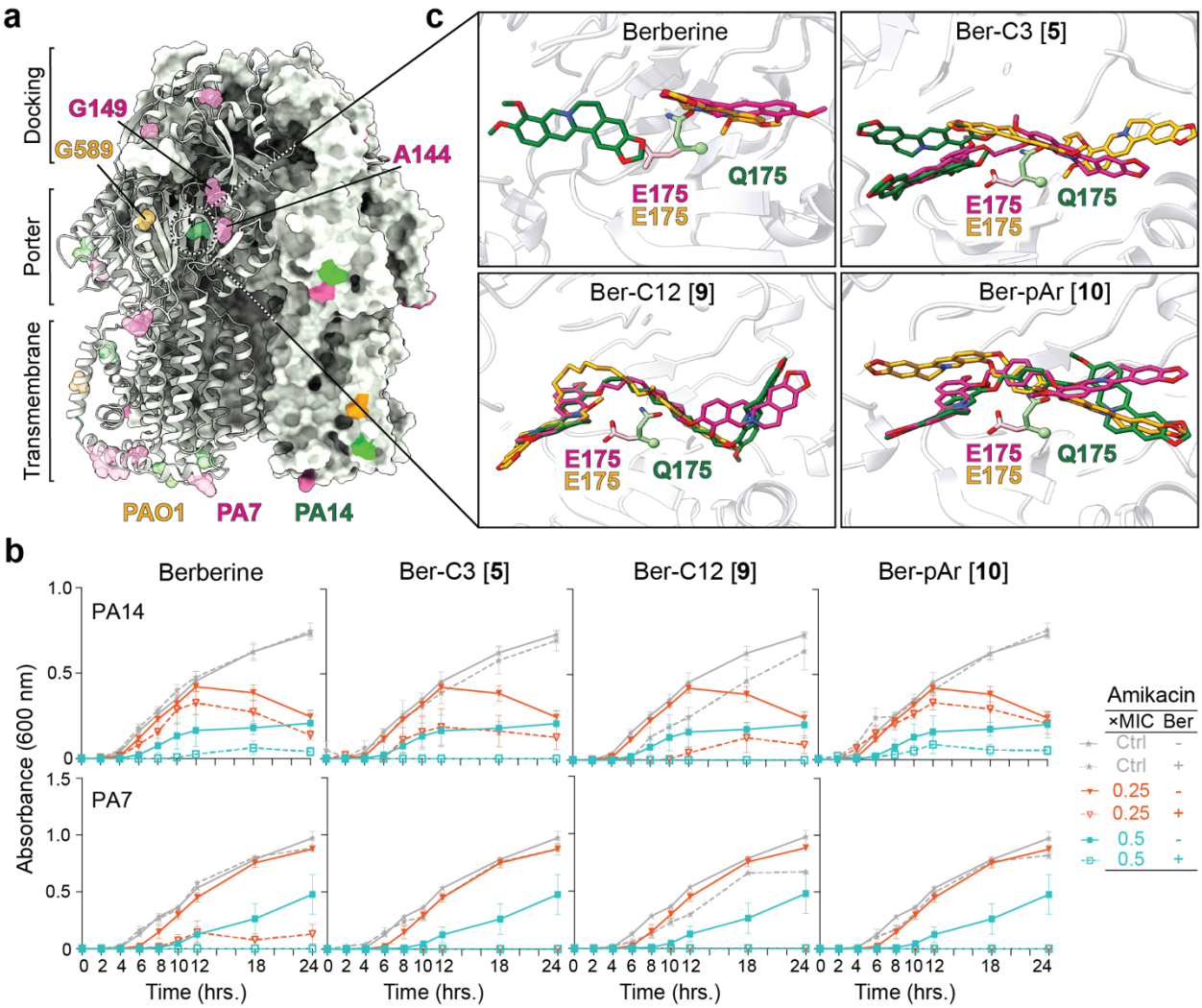

Fig. 5. Berberine and berberine dimers are active against *P. aeruginosa* PA7 and PA14. (a) Unique residues identified from alignment of MexY sequences from *P. aeruginosa* PAO1 (orange), PA7 (pink), and PA14 (green) mapped on a cartoon schematic of $MexY^{PAO1}$ in the binding state. The three domains of the MexY transporter (docking, porter, and transmembrane) are indicated. **(b)** Time-kill assays for berberine and dimer analogs at 64 µg/mL performed over 18 hours in both *P. aeruginosa* PA14 (top) and PA7 (bottom). Synergy was observed in *P. aeruginosa* PA14 with Gen for Ber-C3 [**5**] and Ber-C12 [**9**] which reduced the MIC two-fold (teal open square) compared to no berberine dimer present (teal filled square). In *P. aeruginosa* PA7, all dimer ligands tested reduced the MIC, at minimum, four-fold (red open triangle) at the tested concentration compared to no berberine dimer (red filled triangle). No significant aminoglycoside-independent growth inhibition was observed for berberine or any berberine dimer (dashed grey line) compared to the no antibiotic growth control (grey line). Data shown are the average OD_{600} measurement with error bars representing the standard deviation. **(c)** A zoomed in view of E175 conformation in $MexY^{PAO1}$ (orange) and $MexY^{PA7}$ (pink) which permits binding of berberine (top left), Ber-C3 [**5**] (top right), Ber-pAr [**10**] (bottom left), and Ber-C12 [**9**] (bottom right) in the DBP. In contrast, steric hinderance due to the Q175 conformation in $MexX^{PA14}$ results in altered predicted ligand to bind in this region.